THE GEOLOGICAL SOCIETY
OF AMERICA®

Controls on erosion in the western Tarim Basin: Implications for the uplift of northwest Tibet and the Pamir

Peter D. Clift[1,2], Hongbo Zheng[3], Andrew Carter[4], Philipp Böning[5], Tara N. Jonell[1], Hannah Schorr[1], Xin Shan[6], Katharina Pahnke[5], Xiaochun Wei[7], and Tammy Rittenour[8]

[1]Department of Geology and Geophysics, Louisiana State University, Baton Rouge, Louisiana 70803, USA
[2]School of Geography Science, Nanjing Normal University, Nanjing 210023, China
[3]Research Center for Earth System Science, Yunnan University, Kunming 650091, China
[4]Department of Earth and Planetary Sciences, Birkbeck College, London WC1E 7HX, UK
[5]Max Planck Research Group for Marine Isotope Geochemistry, Institute for Chemistry and Biology of the Marine Environment (ICBM), University of Oldenburg, 26129 Oldenburg, Germany
[6]Key Laboratory of Marine Sedimentology and Environmental Geology, First Institute of Oceanography, State Oceanic Administration, Qingdao 266061, Shandong, China
[7]School of Earth Sciences and Engineering, Nanjing University, Nanjing 210023, China
[8]Department of Geology, Utah State University, Logan, Utah 84322, USA

ABSTRACT

We present here bulk sediment major element chemistry, Nd and Sr isotope ratios, and detrital apatite fission-track (AFT) and U-Pb zircon ages to characterize the provenance of the southwestern Taklimakan Desert (northwest China) and the three major rivers draining this region. We establish the spatial and temporal controls on erosion and sediment transport in the modern Tibetan rain shadow. The Hotan River drains the North Kunlun block and is characterized by zircon populations at 160–230 Ma and 370–520 Ma. The Yarkand River shares these grains with the Hotan, but also has a very prominent zircon population at 40–160 Ma, which is common in Karakoram basement, indicating heavy sediment flux from these ranges to that drainage. This implies a strong control on erosion by topographic steepness and precipitation mediated through glaciation. Our zircon data confirm earlier studies that indicated that the Taklimakan sand is derived from both the Kunlun and Pamir Mountains. AFT ages are younger in the Hotan River than in the Kashgar River, which drains the Pamir, and in both are younger than in the Transhimalaya and parts of the western edge of the Tibetan Plateau. Exhumation is estimated at ~1000 m/m.y. in the North Kunlun and ~500 m/m.y. in the eastern Pamir, which have been exhuming more slowly than the western ranges in the recent past.

Holocene aggradation terracing was dated using quartz optically stimulated luminescence methods and is mostly associated with times of fluctuating climate after 4 ka, with phases of valley filling dated at 2.6, 1.4, and 0.4 ka. The heights and volumes of the terraces show that sediment storage in the mountains is not a significant buffer to sediment transport, in contrast to the more monsoonal Indus system directly to the south. South of the Mazatag Ridge a significant eolian deposit accumulated ~500 yr ago, but this has been deflated in more recent times.

Comparison of the modern river data with those previously measured from Cenozoic foreland sedimentary rocks shows that no sediment similar to that of the modern Yarkand River is seen in the geologic record, which is inferred to be younger than 11 Ma, and probably much less. Uplift of the North Kunlun had started by ca. 17 Ma, somewhat after that of the Pamir and Songpan Garze of northwestern Tibet, dated to before 24 Ma. Sediment from the Kunlun reached the foreland basin between 14 and 11 Ma. North Kunlun exhumation accelerated before 3.7 Ma, likely linked to faster rock uplift.

■ INTRODUCTION

Sediments eroded from mountain chains can potentially provide a relatively continuous record of how such mountains develop, long after the bedrock sources themselves have been eroded away. These sedimentary records allow us to understand whether feedbacks exist between climate, surface processes, and the tectonic evolution of the mountains and provide a key complement to the study of the bedrock sources. Climate-tectonic interactions have been investigated in the Himalaya, the Cascades (northwestern United States), Taiwan, and other regions where precipitation is relatively high and where a link between precipitation and erosion has been established over a variety of time scales (Clift et al., 2008; Dadson et al., 2003; Reiners et al., 2003; Whipple, 2009; Wobus et al., 2003).

Establishing if there is a potential linkage between precipitation and erosion becomes more complicated in regions where rainfall is limited but that host significant amounts of deposited sediments. In these cases, other processes, such as rock uplift or seismic shaking, may dominate in controlling erosion (Burbank et al., 2003; Wallis et al., 2016), although this remains unresolved. In this study we address whether solid Earth tectonic forces, precipitation, or topography are controlling the patterns and rates of erosion around the western Tarim Basin (western China). In this area, rivers are eroding sediment from the Tian Shan, Pamir, and Kunlun and delivering it to the central parts of the basin to the north and east (Fig. 1). We target three neighboring river catchments that have contrasting characteristics that allow these factors in controlling erosion to be assessed. One river is more seismically active (Kashgar River), one drains steep, glaciated terrain with more precipitation (Yarkand
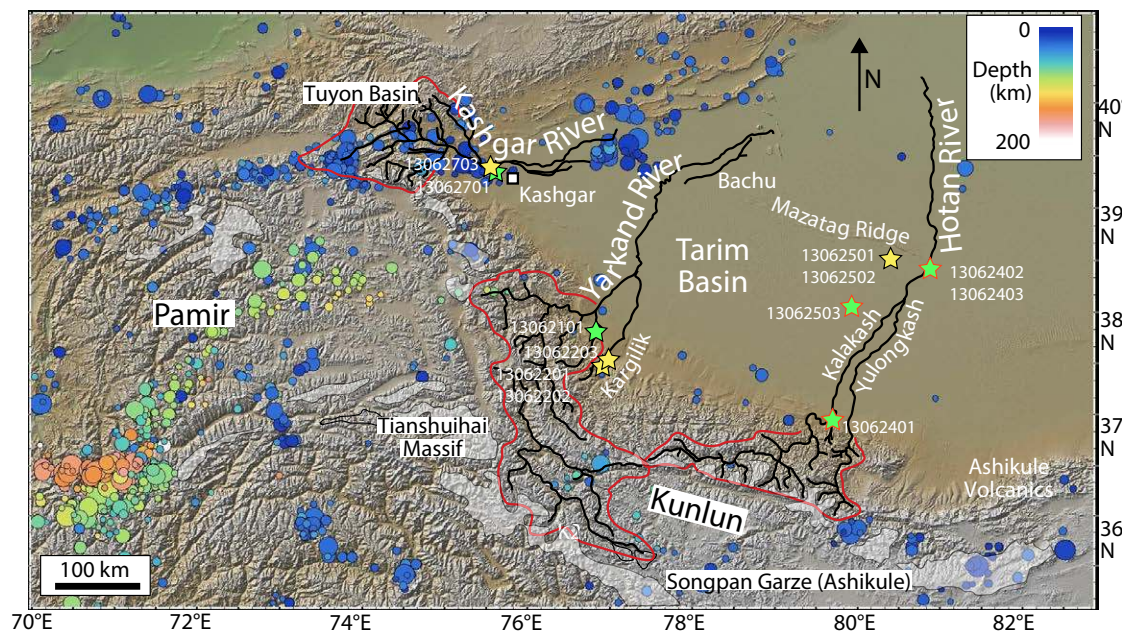
Figure 1. Shaded topographic map of the western Tarim Basin showing the locations sampled for this study. Topographic data are Shuttle Radar Topography Mission data plotted by GeoMapApp software. Earthquake locations are shown from the U.S. Geological Survey catalogue, magnitude 5 and greater (larger dots indicate larger magnitude). Depths of earthquakes are shown by colored scale. Yellow stars show optically stimulated luminescence sampling locations. Green stars show locations of samples with geochemical data and U-Pb zircon dates; green stars with red outlines show locations of samples that also have apatite fission-track data. Black lines show the river networks targeted in this study, with the red lines showing the boundaries of these catchments in the mountains. White shaded regions show the extent of major glaciers.

River), and one is limited to the drier, lower-elevation ranges of the northern Kunlun (Hotan River). Furthermore, changes in bedrock characteristics within the Kashgar and Yarkand Rivers mean that the locus of strongest erosion within those basins can be identified and then related to lateral changes in precipitation, topography, and rock uplift.

Compared to the southern side of the Tibetan Plateau, the northern margin is drier, and precipitation is believed to be mostly brought by the Westerly Jet from moisture sources as far afield as the Mediterranean but with some input from the South Asian monsoon (Böthe et al., 2012; Karim and Veizer, 2002). The Tarim Basin is the location of one of the largest deserts in Asia, the Taklimakan Desert, which is a major source of dust to the atmosphere and plays a significant role in modulating global climate on various time scales (Shao et al., 2011; Uno et al., 2009). Constraining its (Taklimakan Desert) origin is important for both Asian and global climate systems because of its role as a major supplier of aerosols to the atmosphere. We investigated the conclusions of Rittner et al. (2016) that the bulk of the desert sediment is coming from the Pamir and the Kunlun Shan, and not sourced from the Tian Shan.

In this study we analyzed sediments from three major rivers feeding the Tarim Basin using a variety of geochemical (major and trace element compositions, Sr and Nd isotope ratios), geochronological (U-Pb zircon dating), and thermochronological (apatite fission tracks) methods to examine from where sediments are derived within each catchment. We do this to understand what processes might be controlling erosion in this relatively dry but tectonically active environment. Each river has its own unique geographic setting, with the Kashgar River draining the eastern Pamir, the Yarkand River draining the northern Karakoram and Kunlun, while the Hotan River receives material mostly from the northern Kunlun alone (Fig. 2). By better understanding what is controlling modern erosion in these rivers, we constrain how the ancient stratigraphic record can be used to reconstruct the evolving erosion and uplift of the northwestern Tibetan Plateau, building on earlier studies of the exposed Cenozoic sequences (Cao et al., 2014; Sun et al., 2016; Zheng et al., 2000, 2010). Although long understood to be much younger than the topographic uplift of southern Tibet (Tapponnier et al., 2002), the uplift history of the northern plateau remains controversial, yet it is agreed that the development of its present high altitude has important impacts on the development of the Asian monsoon system (Kutzbach et al., 1993; Molnar et al., 1993; Tada et al., 2016; Zhang et al., 2015). Better documentation of the uplift history of the northern Tibetan Plateau is required in order to constrain its role in controlling continental climate regimes.

We also examine the role of climate in buffering sediment flux over millennial time scales through the storage of sediment in valley fills and its release during episodes of incision and the formation of alluvial terraces downstream. In the monsoon-dominated Himalaya, such terracing is driven by changes in precipitation, with more sediment supply and valley filling during wetter times and incision during drier periods (Bookhagen et al., 2006). Here we test to see whether the same relationship holds in a much drier, weakly monsoonal climate.
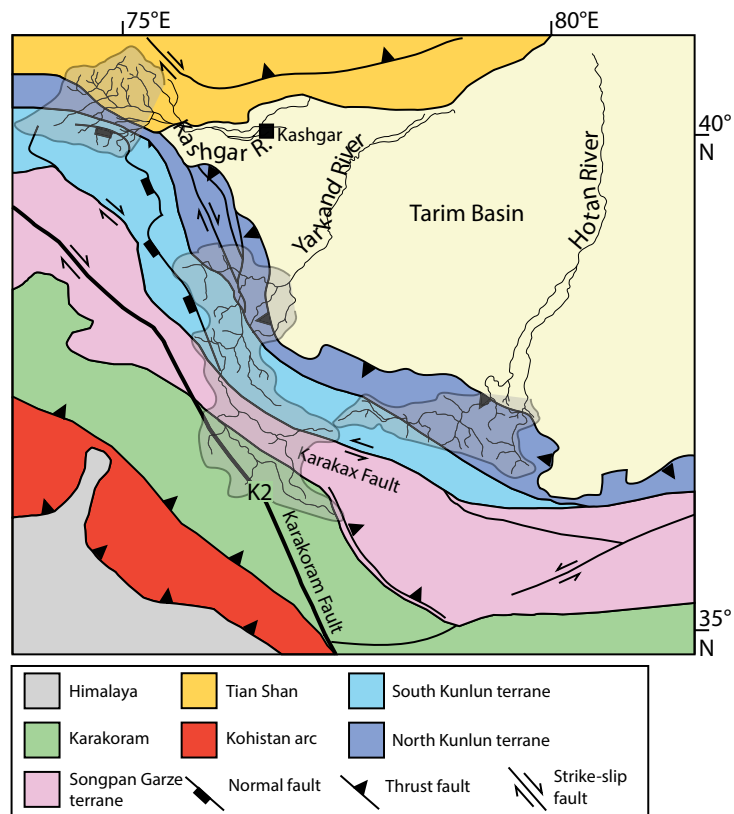
Figure 2. Tectonic map of the major blocks around the western Tarim Basin and the Pamir. Modified after Robinson et al. (2004). Black lines show the river networks targeted in this study, with gray shading indicating the extent of the catchment in the headwaters. The sediments of the modern desert are shown as light yellow.

■ GEOLOGICAL SETTING

Plate Tectonic Setting

The Tarim Basin represents a relatively stable tectonic block within the otherwise strongly deforming zones of western China and northwest Tibet. Mountain building in this region is usually interpreted as a direct response to India-Asia collision, starting sometime during the Paleogene. The exact timing remains controversial (Aitchison et al., 2007; Najman et al., 2010), although there is increasing evidence that uplift may have begun much earlier than was originally conceived (Kapp et al., 2005; Wang et al., 2012). The Tarim Basin is surrounded by a number of tectonic blocks, which have been assembled as a result of subduction predating the final India-Asia collision. Many of these

blocks were rifted from Gondwana and subsequently accreted to the southern margin of Asia during the late Paleozoic–Mesozoic as a result of closure of the Paleo- and then Neotethys Oceans (Sengor and Natal'in, 1996; Yin and Harrison, 2000).

Mountain uplift has radically changed the topography and style of sedimentation across the area (Tada et al., 2010). From latest Cretaceous to early Paleogene, much of the western Tarim Basin was covered by a shallow sea, part of the Paratethys, an epicontinental sea found across much of central Asia, which began to retreat during the Eocene (Bosboom et al., 2011; Schulz et al., 2005). Shallow marine strata of this age are observed along the southwestern margins of the Tarim Basin where they are overlain by a series of clastic sedimentary rocks apparently eroded from the Kunlun to the south and now deformed into a series of thrust sheets that form the frontal ranges of the Kunlun (Cao et al., 2014; Zheng et al., 2000, 2010).

Major Tectonic Blocks

Each of the major ranges that contribute sediment to the rivers and Taklimakan Desert discussed here has its own unique history that allows its erosional products to be identified and quantified in a mixed sediment. The Tian Shan and Kunlun are formed as a result of crustal thickening, with some localized strike-slip faulting (Avouac and Tapponnier, 1993). Sobel and Dumitru (1997) argued that thrusting became the dominant mode of deformation by ca. 25–20 Ma across the region, spanning the Pamir and Kunlun to the Tian Shan. The Pamir form a large, arcuate, north-propagating mountain belt that represents the along-strike equivalent of units found in the Karakoram and western Tibet (Robinson et al., 2004). This range is particularly well known as an example of ongoing continental subduction of Asian lithosphere toward the south under the Indian plate (Burtman and Molnar, 1993) and may represent a younger tectonic process not directly linked to initial India-Asia collision. The northern Pamir have been interpreted as a composite Paleozoic arc terrane correlative to the North and South Kunlun terranes of the western Kunlun Shan (Fig. 2) (Boulin, 1988; Kapp et al., 2007; Tapponnier et al., 1981; Yin and Harrison, 2000). Nonetheless, direct correlation between the Pamir and Tibetan Plateau is still controversial. The Pamir differ from the Himalaya and Tibet in the relative abundance of metamorphic domes that are especially common in the western Pamir but are also found to a lesser extent in the western parts of our field area in the Kunlun south of the city of Kashgar (Burtman and Molnar, 1993; Robinson et al., 2012). The Pamir domes are larger than those documented in Tibet and are dated as Cenozoic in their exhumation, which was especially rapid during the Miocene (Hubbard et al., 1999; Robinson et al., 2007).

The Karakoram represent a complicated tectonic block composed of Mesozoic–Cenozoic metamorphic rocks, as well as limited amounts of sedimentary rocks (Searle, 1991), together with a large Miocene batholith that intrudes the sequence and is associated with post–India-Eurasia collisional melting (Searle et al., 1989). The early magmatic history of the Karakoram involves Cretaceous

intrusive rocks related to an active continental margin along the southern margin of Asia (Searle et al., 1990), possibly equivalent to the Gangdese batholith in central south Tibet. The Karakoram are cut by a major strike slip fault whose timing and degree of motion have been controversial (Murphy et al., 2000; Peltzer and Tapponnier, 1988; Phillips et al., 2004). However, it is clear that this structure is right-lateral and documented to drive rapid rock uplift and exhumation to the present day in central parts of the Karakoram (Foster et al., 1994; Searle and Phillips, 2007), which form the southern edge of the Yarkand catchment.

◼ METHODOLOGY

Each of the tectonic blocks mentioned above has its own unique geological history, which we can exploit to trace from where the sediments in the modern rivers are derived. The wide variety of rock compositions of different ages from each tectonic block (Fig. 3) produces mineral phases that contain unique chemistry and ages. When we analyze these in the modern river sediments, we have the chance to constrain the relative contribution that each block makes to the total sediment flux for each particular river. In doing so we can isolate regions producing the most sediment and thus determine what processes might control our observed rates of erosion.

We choose to employ bulk sediment Sr and Nd isotopes to determine the overall provenance of the sediment. Neodymium is a robust provenance proxy because this element is generally immobile during weathering and erosion (Goldstein et al., 1984). Furthermore, recent work has shown that the Nd content of sediment is largely controlled by the Nd-bearing phases monazite and allanite, which are not separated by density-related mineral sorting during transport and so can be considered immune to hydrodynamic processes (Garçon et al., 2013, 2014). In contrast, Sr isotopes may be more susceptible to change during transport and are also affected by chemical weathering and the presence of carbonate (Derry and France-Lanord, 1996). These caveats make Sr isotope compositions a less reliable provenance tool, but using them in combination with Nd isotopes can be effective. In addition, we use bulk sediment major element compositions to quantify the degree of chemical alteration as an independent technique to assess Sr isotope values and, to a lesser degree, sediment provenance.

Our analysis hinges on thermochronology of single detrital grains because these can identify and quantify individual end-member sources that are obscured in the bulk analysis. Detrital zircon U-Pb dating has become a popular and effective technique for evaluating sediment provenance in clastic systems because zircon is a common mineral in continental rocks and is chemically and mechanically durable enough to survive multiple cycles of erosion, transport, and sedimentation (Gehrels, 2014). Spot size of the laser employed limited analysis to grains >50 μm across. Yang et al. (2012) demonstrated that younger zircons were larger and/or more variable in size than older zircons in the Yangtze River, indicating a potential influence of transport on zircon size and age. Nonetheless, these authors concluded that the 63–125 μm size frac-
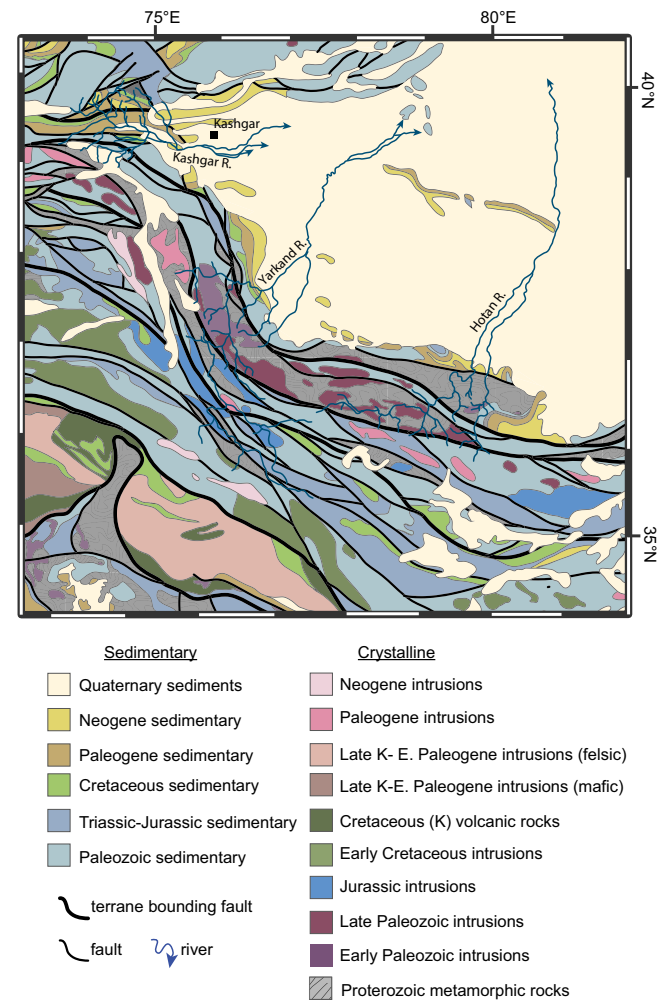
Figure 3. Geological map of the western Tarim Basin, Kunlun, and eastern Pamir showing the potential source regions of sediment into the basin. Terrane-bounding faults from Figure 2 are shown in heavier line weight. K—Cretaceous, E.—Early.

tion yielded almost the same age distribution as the total zircon population, and accurately represents all significant age populations. Our analysis of the 63–125 μm fraction is thus representative of the bulk composition. Given that the rivers examined here are much shorter than the Yangtze (~170 km between the headwaters and the sample point in the Kashgar, ~450 km in the Yarkand, and ~150 km in the Hotan), grain size effects would be less significant because there would be less abrasion of zircon during shorter transport.

We also employ apatite fission-track thermochronology of detrital grains, when apatite was present in sufficient quantities, as a provenance proxy and to constrain rates of exhumation in the source regions. The low-temperature apatite fission-track method records cooling through ~60–125 °C over time scales of 1–10 m.y. (Green, 1989), so is particularly sensitive to exhumation driven by erosion and has been widely used in exhumation studies worldwide, including in northern Tibet (Duvall et al., 2012; Jolivet et al., 2001), the Pamir (Lukens et al., 2012; Sobel et al., 2006a, 2006b), and the Tian Shan (Sobel and Dumitru, 1997; Tang et al., 2015).

We also attempt to examine how Quaternary climate change may have impacted sediment transport, and to do this we sample fluvial terraces found within the valleys feeding the south side of the Tarim Basin, as well as from selected aeolian deposits within the Tarim Basin itself. Age control for Holocene deposits was determined using optically stimulated luminescence (OSL) dating of quartz in sediments. This technique dates the last time the sediment was exposed to sunlight, presumably during transport. It is widely applied to quartz-bearing sediment, largely deposited in the past 200 k.y. (Rhodes, 2011).

■ SAMPLING

Samples were taken for provenance and OSL dating from along the southwestern edge of the Tarim Basin. Sample locations are shown in Figure 1 and are listed in Table 1. Sediments containing fine to medium sand (>63 μm) were preferentially sampled for provenance analysis. This size fraction is ideal for single-grain mineral provenance techniques that are limited by an analytical laser spot size of >50 μm. We recognize that by only analyzing the >63 μm sediment we are not including the suspended load which may have a different provenance, possibly introducing bias to the bulk sediment provenance interpretation (Garzanti et al., 2011). However, our data are derived from a wide array of grain sizes >63 μm, which we argue contributes to an initial constraint on sediment generation patterns in this region.

Three proximal river sands from the Kashgar (sample 13062701), Yarkand (13062101), and Hotan (13062401) Rivers were sampled near where they leave their mountain source areas to quantify the sediment being produced in the ranges and before any significant recycling of older sediment within the flood plains were to be incorporated. The Hotan was sampled from its larger, western Kalakash River branch. These samples were chosen because the Kashgar River, draining ~11,000 km², is the largest river draining the Pamir into the Tarim Basin, while the Hotan River allows us to assess the erosion flux from ~12,500 km² of the North Kunlun (Fig. 2). In contrast, the Yarkand drains ~25,000 km² as far south as the Karakoram and permits us to quantify what their (the Karakoram) contribution has been to sediment flux into the Tarim Basin. Samples were taken directly from the banks of the active stream where the sediment had clearly been recently transported.

Sample 13062403 was taken from the Hotan River in the center of the Tarim Basin to assess how much recycling of sediment from the Taklimakan Desert into the river had occurred and to what extent the erosional signal from the upper Hotan is propagated into the basin. Sample 13062402 was taken from the sand dunes immediately adjacent to the Hotan River next to Sample 13062403. Sample 13062503 was taken from a dune within a major sand sea in the central part of the basin, south of the Mazatag Ridge (Fig. 1), in order to characterize the origin of the sediment in that part of the desert and test the proposed dominant provenance in the Pamir and the Kunlun (Rittner et al., 2016). Although eolian sand may have experienced more reworking than the more proximal fluvial sediments, it is still possible to assess provenance using the same methods.

Samples for OSL dating were taken from two regions. South of the Mazatag Ridge there are a series of prominent sediment mounds with Euphrates poplar trees growing on their summits (Figs. 4A and 4B). Wind-blown silt and sand under these trees are fixed and buffered from transport by well-established root systems. These sediment mounds overlie older meandering river sediment, which suggests that this area clearly was a region of net deposition for desert sediments. However, in more recent times the region has been

TABLE 1. SAMPLE NUMBERS AND LOCATIONS

Sample number	Location	Sample type	Latitude	Longitude
13062101	Yarkand River	Provenance	37°56.32′N	76°34.542′E
13062201	Kargilik River basin	OSL	37°39.411′N	76°49.454′E
13062202	Kargilik River basin	OSL	37°39.411′N	76°49.454′E
13062203	Kargilik River basin	OSL	37°42.096′N	76°51.670′E
13062401	Upper Hotan River	Provenance	37°5.904′N	79°57.596′E
13062402	Dune sand	Provenance	38°27.229′N	80°52.066′E
13062403	Lower Hotan River	Provenance	38°27.229′N	80°52.066′E
13062501	Mazatag Mounds	OSL	38°37.074′N	80°27.231′E
13062502	Mazatag Mounds	OSL	38°37.112′N	80°27.270′E
13062503	Dune sand	Provenance	38°3.299′N	80°12.164′E
13062701	Kashgar River	Provenance	39°27.886′N	75°52.513′E
13062703	Kashgar River	OSL	39°27.886′N	75°52.513′E

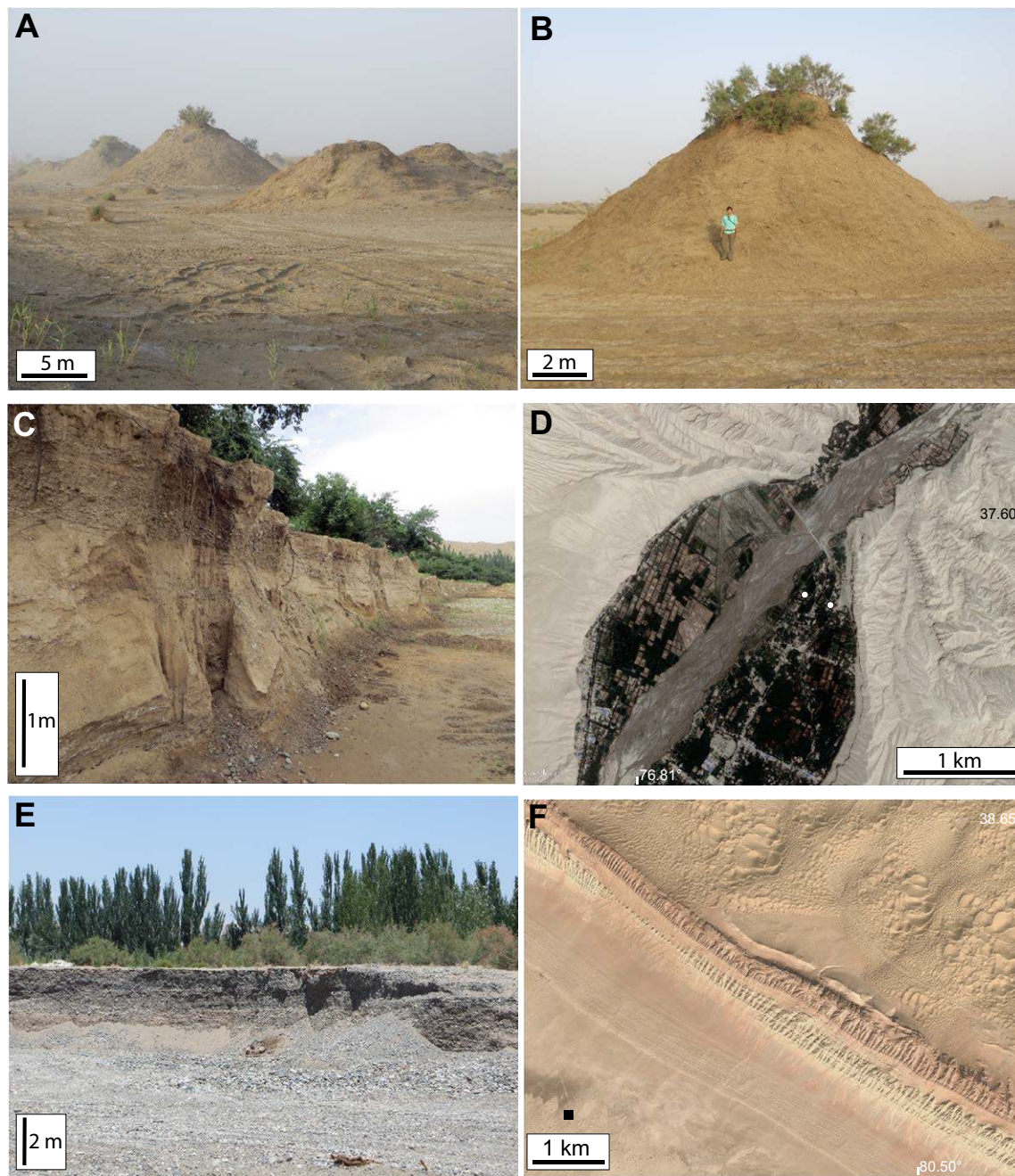*Note:* OSL—optically stimulated luminesence.

Figure 4. Field photographs showing the locations sampled for optically stimulated luminescence dating. (A, B) Mounds of windblown fine sand at Mazatag Ridge with trees stabilizing the top of the sediment (samples 13062501 and 13062502). (C) Fluvial terrace in the Kargilik River joins the Yarkand River in the Tarim Basin (sample 13062201). (D) Aerial photograph from Google Earth of the Kargilik River showing the locations of two terraces sampled upstream from that shown in C (samples 13062202 and 13062203; dots indicate the two sample locations). (E) Fluvial terrace from the Kashgar River just to the west of Kashgar (samples 13062701 and 13062703). (F) Aerial photograph of the Mazatag Ridge showing location of photographs A and B (black square) and the sand sea piled up on the north side.

significantly deflated, leaving only the remnants of the poplar mounds. Sand continues to accumulate on the north side of the Mazatag Ridge (Fig. 4F), implying a change in wind dynamics. Our samples were designed to date the age of accumulation and place a lower boundary on the time of the wind reorganization and deflation.

Aggradational fill terraces along the upper Kargilik River, a tributary to the Yarkand (Fig. 1), were also sampled for OSL dating. Although the Kargilik is not the main stream of the Yarkand, it appears that such terraces are of regional extent and representative of the geomorphology. These terraces rise >15 m above the modern river bed, with at least two lower terrace levels identified in the valley (Figs. 4C and 4D). Although these terraces are now farmed, there is little agricultural disturbance upstream. We sampled here to date times of net valley aggradation and to place a lower bound on the incisional episodes. In addition, we sampled a 4-m-high Kesile River terrace (sample 13062703) immediately west of Kashgar to establish whether timing of aggradation and incision were regionally synchronous between the Pamir and the Kunlun River basins.

■ ANALYTICAL METHODS

Details regarding geochemical, provenance, and OSL analyses are provided in the Supplemental Information[1] and are summarized here. Samples were analyzed for major and trace elements to provide a basic characterization of the material by X-ray fluorescence; the data are presented in Table 2. Sediments were also analyzed for Sr and Nd isotopes because these systems have an established track record of being reliable provenance and chemical-weathering proxies in sedimentary systems (Goldstein et al., 1984). The isotopic compositions of Nd and Sr were analyzed on a Thermo Neptune Plus Multicollector inductively coupled plasma-mass spectrometer (ICP-MS) at the Institute for Chemistry and Biology of the Marine Environment, Oldenburg, Germany. Isotopic results are reported in Table 2. Neodymium isotope analy-

ses were corrected against the JNdi-1 standard. We calculate the parameter ε_{Nd} (DePaolo and Wasserburg, 1976) using a ^{143}Nd/^{144}Nd value of 0.512638 for the chondritic uniform reservoir (Jacobsen and Wasserburg, 1980).

Detrital zircons were dated using the U-Pb method at the London Geochronology Centre facilities at University College London (UK), using a New Wave Nd:YAG 193 nm laser ablation system, coupled to an Agilent 7700 quadrupole ICP-MS. Around 100–120 grains are considered generally sufficient for characterizing sand eroded from a geologically complicated drainage basin (Vermeesch, 2004). Results are presented in Table S1 in the Supplemental Information (see footnote 1).

Depositional ages of sediment in the terraces were determined by OSL dating of quartz sand following the single-aliquot regenerative dose method (Murray and Wintle, 2000). While OSL dating can be challenging in fluvial environments, deposits from these settings can be accurately dated by selecting depositional facies most likely to have been reset by sunlight exposure (Fuchs and Owen, 2008; Rittenour, 2008; Wyshnytzky et al., 2015). We preferentially targeted well-sorted, horizontally bedded sand lenses from fluvial deposits to reduce the influence of incomplete resetting (partial bleaching) of the luminescence signal. Samples were processed at the Utah State University Luminescence Laboratory (Logan, Utah, USA), and results are presented in Table 3. More information on sample processing, analysis, and equivalent dose distributions can be found in the Supplemental Information (see footnote 1).

■ RESULTS

Mineralogy

Samples were predominantly quartz-rich, well-sorted, and sub-angular to sub-rounded sands (Fig. S1 in the Supplemental information [see footnote 1]). It is noteworthy that the desert dune sand sample 13062503 (Fig. S1D [see

TABLE 2. BULK SEDIMENT MAJOR AND TRACE ELEMENT COMPOSITIONS, TOGETHER WITH ASSOCIATED Sr AND Nd ISOTOPE RATIOS

Sample number	Location	SiO$_2$ (%)	TiO$_2$ (%)	Al$_2$O$_3$ (%)	Fe$_2$O$_3$ (%)	MnO (%)	MgO (%)	CaO (%)	Na$_2$O (%)	K$_2$O (%)	P$_2$O$_5$ (%)	As (ppm)	Ba (ppm)	Ce (ppm)	Co (ppm)	Cr (ppm)	Cu (ppm)	Ga (ppm)
13062101	Yarkand River	64.4	0.33	11.3	2.54	0.045	1.91	7.73	2.56	2.35	0.1	5	509	52	6	28	12	13
13062401	Upper Hotan River	69.9	0.49	12.2	3.25	0.079	1.57	3.88	2.57	2.7	0.17	14	354	77	7	51	10	15
13062402	Dune	67.6	0.41	10.6	2.66	0.053	1.84	6.63	2.43	2.2	0.1	5	535	51	7	43	10	10
13062403	Lower Hotan River	66.7	0.50	11.0	3.07	0.061	1.98	6.64	2.49	2.32	0.15	6	456	62	8	54	12	13
13062701	Kashgar River	69.7	0.39	7.3	2.74	0.056	1.25	7.97	1.69	1.22	0.08	5	382	39	6	34	13	7

Sample number	Location	Mo	Ni	Nb	Pb	Rb	Sr	Th	Y	V	U	Zn	Zr	^{87}Sr/^{86}Sr	2σ SD	^{143}Nd/^{144}Nd	εNd	2σ SD
13062101	Yarkand River	0	14	10	17	90	265	8	11	48	6	31	101	0.71427	0.000029	0.512086	−9.9	0.29
13062401	Upper Hotan River	0	25	13	17	142	184	10	21	51	5	47	192	0.72196	0.000025	0.512175	−8.1	0.23
13062402	Dune	0	20	12	16	82	272	9	15	48	6	33	139	0.71843	0.000025	0.512084	−9.9	0.23
13062403	Lower Hotan River	1	24	12	16	99	235	9	23	54	4	41	222	0.71996	0.000025	0.512102	−9.6	0.26
13062701	Kashgar River	0	14	9	12	38	230	5	10	47	7	34	173	0.71172	0.000025	0.512158	−8.5	0.25

Note: Explanation of methods used to obtain this data is in the Supplemental Information (see text footnote 1). SD—standard deviation.

TABLE 3. DATA AND DEPOSITIONAL AGES FROM THE OPTICALLY STIMULATED LUMINESCENCE (OSL) ANALYSIS OF TERRACE SEDIMENTS

Sample number	Location	Number of aliquots*	Depth (m)	U (ppm)	Th (ppm)	K (%)	Rb (ppm)	Cosmic contribution (Gy/k.y.)[†]	Dose rate (Gy/k.y.)[§]	Equivalent dose, De (Gy)[#]	OSL age (ka) ± 2 σ
13062201	Kargilik River	19 (37)	1.50	2.4 ± 1.7	10.5 ± 1.0	1.88 ± 0.05	96.6 ± 3.9	0.21 ± 0.02	3.26 ± 0.17	1.36 ± 0.61	0.42 ± 0.19
13062202	Kargilik River	19 (45)	2.00	2.6 ± 0.2	12.4 ± 1.1	1.75 ± 0.04	88.0 ± 3.5	0.20 ± 0.02	3.29 ± 0.18	8.47 ± 1.26**	2.57 ± 0.46
13062203	Kargilik River	17 (47)	1.00	2.2 ± 0.2	10.5 ± 1.0	1.70 ± 0.04	82.8 ± 3.3	0.23 ± 0.02	3.06 ± 0.16	4.27 ± 1.33	1.40 ± 0.46
13062501	Mazatag Mounds	8 (43)	2.50	2.2 ± 0.2	9.5 ± 0.9	1.66 ± 0.04	77.6 ± 3.1	0.17 ± 0.02	2.88 ± 0.16	1.44 ± 0.56**	0.50 ± 0.20
13062502	Mazatag Mounds	13 (34)	1.70	2.2 ± 0.2	10.3 ± 0.9	1.63 ± 0.04	76.3 ± 3.1	0.18 ± 0.02	2.93 ± 0.16	1.50 ± 0.49[††]	0.51 ± 0.18
13062703	Kashgar River	26 (35)	1.25	1.1 ± 0.1	4.5 ± 0.4	1.07 ± 0.03	44.9 ± 1.8	0.20 ± 0.02	1.74 ± 0.09	4.81 ± 2.11	2.76 ± 1.24

Note: Samples analyzed following the single-aliquot regenerative-dose method (Murray and Wintle, 2000). See Supplemental Information (text footnote 1) for more information.

*Number of aliquots used for age calculation; number of aliquots measured in parentheses. Rejection of aliquots follows standard rejection criteria.

[†]Contribution of cosmic radiation to the dose rate was calculated by using sample depth, elevation, and longitude and latitude following Prescott and Hutton (1994).

[§]Total dose rate to quartz assumes 3 ± 3 wt% H_2O content of the sediments.

[#]Equivalent dose (De) calculated using the minimum age model (MAM) of Galbraith and Roberts (2012) unless noted otherwise. Error on De is 2σ standard error.

**De calculated using the central age model of Galbraith and Roberts (2012).

[††]De calculated using the mean of the De data.

Figure 5. (A) Q-F-L (Quartz-feldspar-lithic) ternary provenance discrimination diagrams of point counts of point counting data of grain mineral type. Diagrams indicate a dominantly recycled orogenic source terrane. Ternary diagram and fields modified from Dickinson et al. (1983). (B) A-CN-K [Al_2O_3-(CaO + Na_2O)-K_2)] plot of Fedo et al. (1995) showing extremely low chemical index of alteration (CIA) values for all samples. Y—Yarkand River (sample 13062101); uH—upper Hotan River (13062401); lH—lower Hotan River (13062403); K—Kashgar River (13062701); D—dune sand from near the Hotan River (13062402). kao—kaolinite; chl—chlorite; gb—gibbsite; sm—smectite; il—illite; m—muscovite; bi—biotite; ksp—K-feldspar; pl—plagioclase.
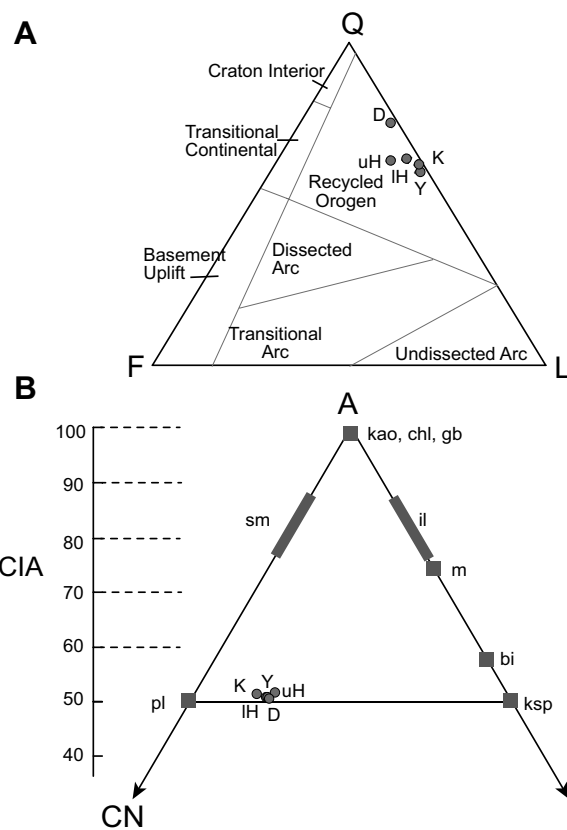
footnote 1]) does not show a particularly rounded morphology, indicating that these sediments may not have been recycled within the desert for a long time. However, this sample is richer in quartz compared to other analyzed sands. There is a significant minority population of mafic heavy minerals and lithic fragments, particularly metamorphic rock fragments, in all samples that dominate compared to volcanic lithic grains, although carbonate grains are also present, except in the upper Hotan River (sample 13062401). Quartz tends to be monocrystalline, although with a significant subpopulation of polycrystalline, metamorphic quartz. The provenance sample from the Kashgar River (13062701) is noteworthy in having a particularly high proportion of chert fragments. When plotted on the Quartz-Feldspar-Lithic diagram of Ingersoll et al. (1984), the sands plot within the recycled orogenic field (Fig. 5A).

Bulk Sediment Chemistry

Bulk sediment chemistry reveals a relatively normal, quartz-rich continental sand composition for all samples. On the A-CN-K [Al_2O_3-(CaO+Na_2O)-K_2O] plot of Fedo et al. (1995), the samples plot toward the CN (CaO+Na_2O) axis and show very low chemical index of alteration values using the equation of Nesbitt et al. (1980) (Fig. 5B). This indicates that the sediments are very weakly altered compared to their bedrock source, despite their apparent recycled orogenic assignment. Radiogenic isotopes show a limited range in Nd isotope composition, with ε_{Nd} values spanning –8.1 to –9.9, while $^{87}Sr/^{86}Sr$ values are quite widely dispersed between 0.71171 (Kashgar River) and 0.72195 (upper Hotan River) (Fig. 6).

Apatite Fission-Track Dating

Because of insufficient apatite, only three samples could be analyzed for apatite fission tracks to constrain both provenance and regional exhumation rates. The analyses were performed at University College, London (UK), with

Clift et al. | Controls on erosion in the western Tarim Basin
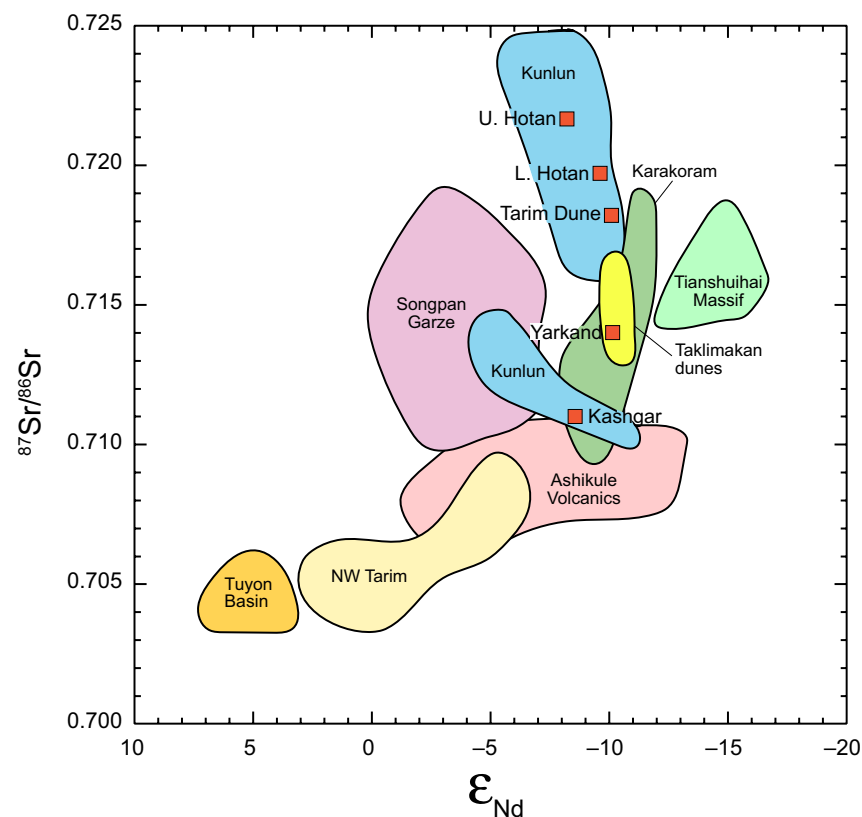
Figure 6. Sr isotope ratios plotted against ϵ_{Nd} values for modern sediments from the Hotan, Yarkand, and Kashgar Rivers and from dune sands in the Tarim Basin. We also show the range of possible basement source rocks in the western Tarim Basin. Fields are defined from source data from GEOROC (Geochemistry of Rocks of the Oceans and Continents; http://georoc .mpch-mainz.gwdg.de/georoc/), except for Songpan Garze turbidite sandstones which are from She et al. (2006), Karakoram data from Schärer et al. (1990), Kunlun terrane data from Robinson et al. (2012) and Chang et al. (2000), and Taklimakan Desert sands from Chang et al. (2000). U.—upper; L.—lower.

the results presented in Table S2 (see footnote 1) and in Figure 7. The upper Hotan River sample (13062401) shows a dominant young age peak at 3.7 ± 0.4 Ma, with a central age of just 9.9 Ma. Two other peaks are noted at 17.3 and 107 Ma, but these are much less abundant. The lower Hotan sample (13062403) yielded a less well-defined but similar age spectrum, with a central age of 28 ± 7.4 Ma and a prominent younger population detected at 5.3 ± 0.9 Ma. The dune sand has the oldest fission-track ages with a central age of 37.3 ± 7.5 Ma and a prominent peak of 8.1 ± 0.9 Ma, as well as two older populations clustered at 30.8 and 178 Ma.

U-Pb Zircon Dating

Four of the five sand samples yielded >110 grains for U-Pb dating, which is generally considered to be the threshold for an accurate statistical representation for a sediment derived from a complex source terrain (Vermeesch,

2004). Only the Yarkand sample had significantly fewer than this number (43), and so our inferences based on those data must be considered less reliable. The age spectra for the samples are shown in Figure 8. We identify six prominent age populations that are common to many of the samples: 40–160 Ma, 160–230 Ma, 230–370 Ma, 370–520 Ma, 520–690 Ma, 690–900 Ma, and >900 Ma. There are very few grains older than 900 Ma or younger than 40 Ma. The Yarkand River is distinctive in showing a prominent population at 40–160 Ma that is not found in the other rivers. In contrast, the upper Hotan is unique in having a very abundant 160–230 Ma population, although this group is also seen at lower concentrations in the dune sand and the lower Hotan sample. The Kashgar River has prominent populations at 370–520 Ma and 520–690 Ma and is unique in our data set in having a sizable 690–900 Ma population (Fig. 8). The dune sand and lower Hotan samples have relatively similar age spectra, although the dune sand has a more abundant 230–370 Ma population.
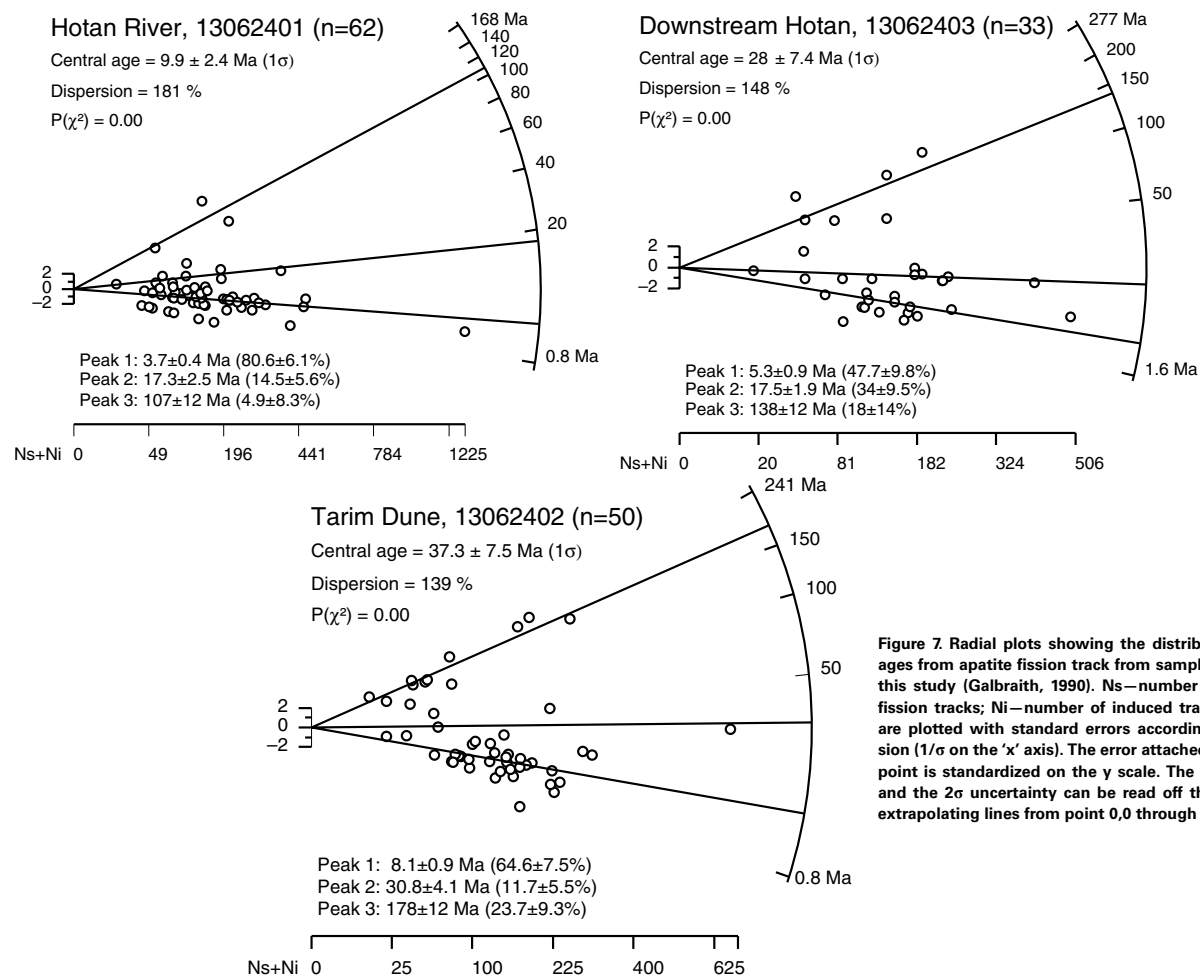
Figure 7. Radial plots showing the distribution of cooling ages from apatite fission track from samples considered in this study (Galbraith, 1990). Ns—number of spontaneous fission tracks; Ni—number of induced tracks. Single ages are plotted with standard errors according to their precision (1/σ on the 'x' axis). The error attached to each plotted point is standardized on the y scale. The value of the age and the 2σ uncertainty can be read off the radial axis by extrapolating lines from point 0,0 through the plotted age.

Optically Stimulated Luminescence

The OSL ages reveal a relatively young set of terraces along the Kargilik River, with the oldest dating to 2.57 ± 0.46 ka and two younger, lower terraces at 1.40 ± 0.46 ka and 0.42 ± 0.19 ka respectively (Table 3). Other young ages of sedimentation are found in the Mazatag Mounds that represent deflated remnants of desert dunes on the south side of Mazatag Range. Depositional ages here are only 0.50 ± 0.20 ka. Finally, the terrace above the Kashgar River near Kashgar provides a depositional age of 2.76 ± 1.24 ka, close to the older terrace age in the Kargilik valley.

◼ DISCUSSION

Sediment Provenance

Bulk Isotope Chemistry

We now use the data presented above to make inferences about the source of sediment in the modern river systems by comparing the new data presented here with existing bedrock data. Figure 6 shows that the upper Hotan River sample (13062401) has a Sr and Nd isotope composition that lies within the
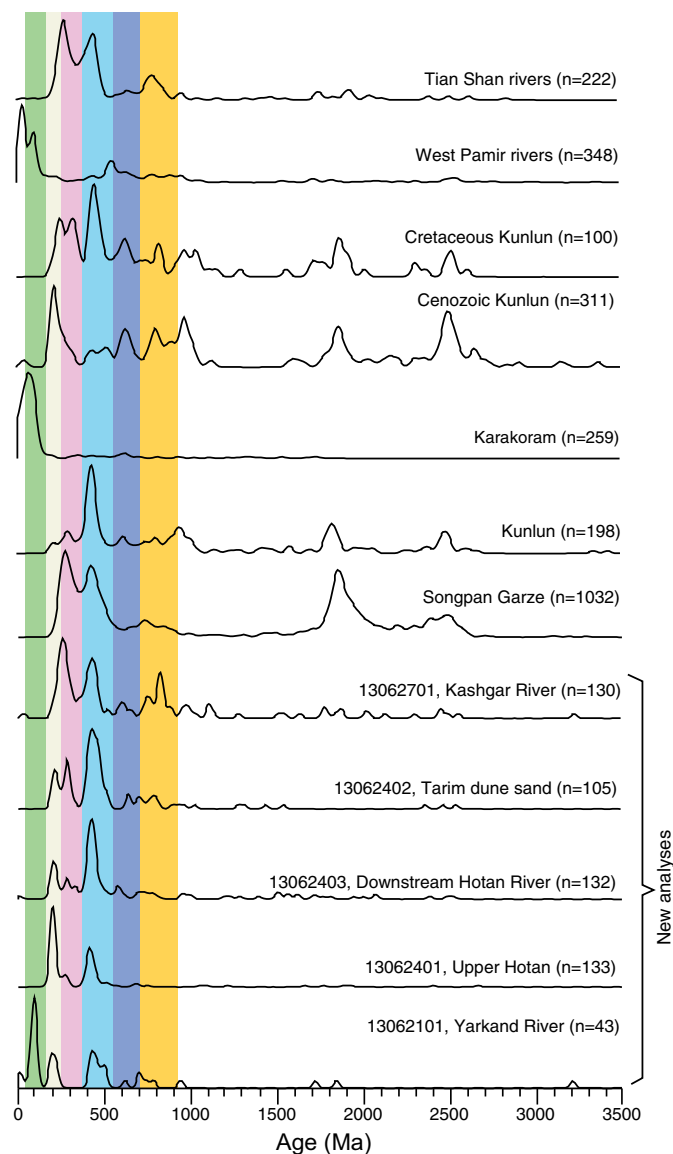
Figure 8. Kernel density estimate plots of zircon U-Pb ages from the samples considered in this study showing the relative abundance of different-aged crystals in each. Vertical color bands show defined U-Pb age populations considered to be of use in source discrimination. Data from Kunlun basement and Cenozoic sediments are from Bershaw et al. (2012). Western Pamir river data are from Lukens et al. (2012). Tian Shan river data are from Rittner et al. (2016). Karakoram data are from the compilation of Clift et al. (2004), together with more recent data from Ravikant et al. (2009). Songpan Garze data are from Weislogel et al. (2010).

range of bedrock and proximal moraine compositions from the Kunlun, albeit with higher-than-average $^{87}Sr/^{86}Sr$ values. This relationship might be expected based on the modern drainage pattern of that river (Fig. 2). In contrast, the Yarkand River sample (13062101) plots at a similar ε_{Nd} value but lower $^{87}Sr/^{86}Sr$ value, within the range of the Karakoram basement values, as well as being close to those of basement of the Tianshuihai Massif. The tectonic zonation map (Fig. 2) indicates that the Tianshuihai Massif is composed of both Karakoram and Songpan Garze terranes. The Sr and Nd data suggest that most of the sediment in the Yarkand is being derived from its upper reaches and not from the northern parts of the catchment closer to the edge of the Tarim Basin itself. The Kashgar River sample (13062701) plots at a lower $^{87}Sr/^{86}Sr$ value again, closer but still above the range of the various volcanic suites of the Ashikule Volcanic Group. The rocks of the Tuyon Basin lie within the Kashgar drainage but have much lower $^{87}Sr/^{86}Sr$ values and higher ε_{Nd} values, indicating that any erosion from those rocks is quite limited. Instead, sediment production appears to be dominated by sources isotopically similar to those supplying the Yarkand River. Not surprisingly, the lower Hotan sample (13062403) and the dune sand sample (13062402) plot close together, consistent with significant reworking of desert sand into the river. The desert sand itself is intermediate between the Hotan and Yarkand samples in Sr and Nd, and has higher $^{87}Sr/^{86}Sr$ values than earlier analyses from the Taklimakan Desert (Chang et al., 2000). Our desert sand data could be explained by erosion from a mixture of Kunlun and Pamir (Kashgar) sources, consistent with the findings of Yang et al. (2007) and Rittner et al. (2016). Our sediment appears to show more Kunlun and less Pamir influence compared to the earlier analyses that were taken along the northern edge of the Tarim Basin. Our Nd and Sr data do permit the possibility that the Karakoram have been a source to the desert, although this is not required.

Zircon U-Pb Evidence

We can explore these conclusions further by consideration of the zircon U-Pb ages. The upper Hotan River is marked by a very prominent population at 160–230 Ma (Fig. 8). This population is not commonly found in the other rivers and given the extent of the drainage must be derived from the Kunlun, likely the North Kunlun terrane (Fig. 2). Although basement samples from this area have not yet shown this peak, this implies inadequate sampling of the basement to date. It is noteworthy that this 160–230 Ma group, although as yet unseen in bedrock analyses, exists as a very prominent population within Cenozoic sedimentary rocks preserved within the Kunlun (Bershaw et al., 2012).

The Yarkand River shares with the Hotan River zircon age populations at 160–230 and 370–520 Ma, which is unsurprising given that this river also drains through the South and North Kunlun. However, the Yarkand contains a very prominent peak at 40–160 Ma, which is not seen in the other rivers but is common in Karakoram basement. This indicates that a large quantity of the sediment in the Yarkand River is derived from the Karakoram, consistent with bulk isotope data and the modern drainage geometry.

The Kashgar River differs from the other rivers in showing a significant 230–370 Ma group, as well as an older 690–900 Ma population, almost unknown in the other rivers or the Taklimakan Desert. The Kashgar River shares the strong 370–520 Ma group with the other studied rivers. This group is well known from basement samples in the Kunlun, which forms the southern side of that drainage, implying erosion from that region. The differences in the observed zircon ages and age frequencies between the Kashgar and Hotan Rivers would thus likely reflect the influence of sources to the north, within the Tian Shan.

As with the bulk isotope data, the downstream Hotan River and the dune sands share a similar pattern in U-Pb zircon ages. These two samples also share several populations with the upstream Hotan and Kashgar Rivers, but not with the Yarkand, implying that this river is not a major source of sediment to the Taklimakan Desert. This may indicate that the flux from the Yarkand is overwhelmed within the Tarim Basin by flux from other rivers, and/or that drainage from the Karakoram to the Tarim Basin has initiated quite recently. Our zircon data are consistent with the work of Rittner et al. (2016) in demonstrating that the Taklimakan dune sand reflects input from both the Kunlun and the Pamir.

Controls on Provenance

What controls the rates of erosion between the different river basins remains problematic because we do not have information on the volumes of material sourced by the Kashgar, Yarkand, and Hotan Rivers. The Kashgar River catchment is easily the most tectonically active (Fig. 1) but is otherwise unremarkable in terms of its topography or precipitation (Fig. 9). The Kashgar appears to be steeper and slightly wetter on its northern side compared to its southern side. Provenance constraints from U-Pb detrital zircons indicate that more sediment is being derived from north of the drainage (Fig. 6), raising both of these factors, topography and precipitation, as possible crucial constraints. The Yarkand River drains the steepest topography, especially in its headwaters close to the Karakoram, where it also experiences relatively high rates of precipitation. The combination of steep local topographic relief and precipitation, which encourages strong glacial development, may be the reason that this part of the catchment is so productive relative to the Kunlun. In contrast, the Hotan River is the driest catchment with only slightly higher rates of precipitation in its western reaches. It is also the most topographically reduced. However, because the Hotan River drains essentially only one major

tectonic block, our data do not allow us to resolve what is controlling the distribution of erosion patterns within this drainage. In the other cases, however, there is a consistent link to climate, and especially precipitation, being the primary control over relative erosion rates within a given basin, even if tectonics is forming the topography against which orographic precipitation is occurring.
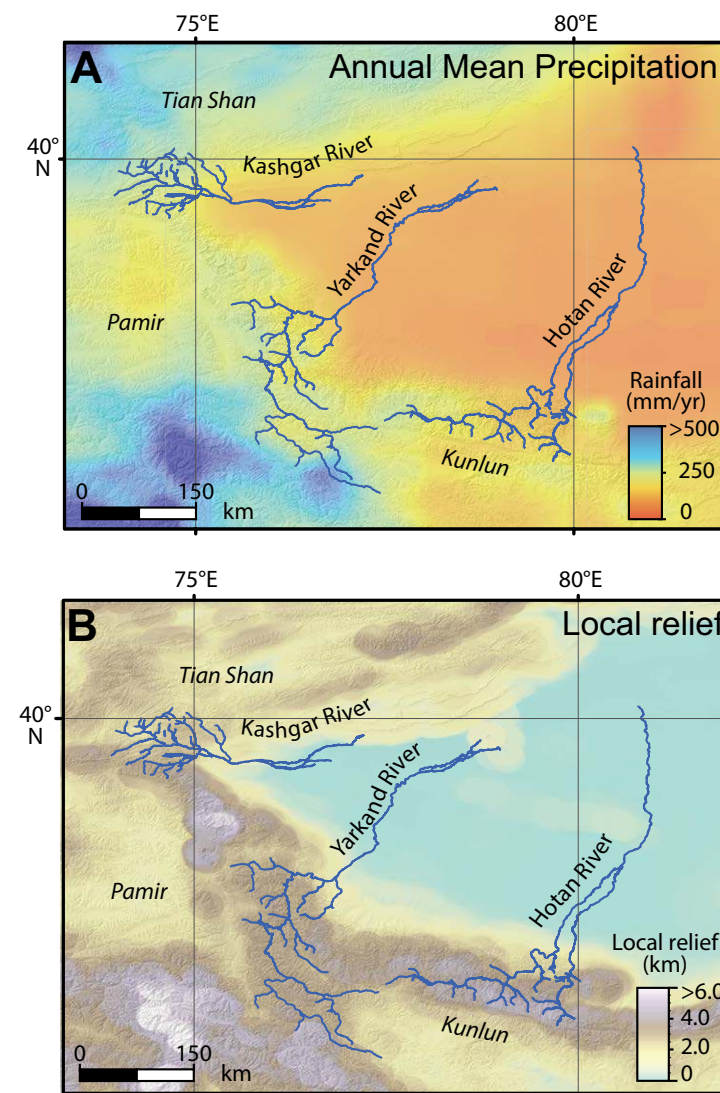
Figure 9. Annual mean rainfall and local topographic relief for the study area. (A) Annual rainfall values derived from Tropical Rainfall Measuring Mission version 3B42 data from A.D. 1998 to 2009 at 0.25° × 0.25° resolution (http://www.geog.ucsb.edu/~bodo/TRMM/). (B) Mean local topographic relief calculated using a 20-km-radius moving window from void-filled Shuttle Radar Topography Mission 1990 Digital Elevation Model. Blue lines denote the stream network.

Paleo-Erosion Patterns

We apply our understanding of the erosion in the modern rivers to interpretation of ancient deposits to better constrain the erosion of the northern edge of the Tibetan Plateau. Cao et al. (2014) published a series of detrital zircon U-Pb ages from a section close to the modern Hotan River and used these to reconstruct the progressive exhumation of the northern edge of the Tibetan Plateau during the Cenozoic. In our reassessment, we assign depositional ages based on the stratigraphic correlation shown in Figure 10 and using the revised ages from Zheng et al. (2015), who employed a slightly different lithostratigraphy. The age of the base of the section is well defined as Eocene, based on marine fossils, while the top of the section, defined as the Xiyu Formation by Zheng et al. (2015), is dated at 11 Ma based on a volcanic ash deposit. We correlate these two sections with the revised depositional ages to aid in our understanding of evolving erosion patterns.

The oldest formation, the Keziluoyi, yielded strong zircon age peaks at ca. 300 and 450 Ma (Fig. 11) that are also observed in the Kashgar River as well as in the desert sands. However, the Keziluoyi Formation lacks the 690–900 Ma population found in the Kashgar River. It seems likely that the Keziluoyi Formation had similar sources to those now supplying the desert sand, implying erosion both from the Pamir and from the Kunlun.

We employ multidimensional scaling (MDS) (Fig. 12) to assess the similarity of ancient and modern sediments and their potential bedrock source terranes (Vermeesch, 2013). MDS is a standard statistical technique similar to principal component analysis, which can be used to create a plot measuring the similarity between sample zircon age spectra much like the Kolmogorov-Smirnov method that quantifies the distance between the empirical cumulative distribution functions of two samples. MDS plot axes are themselves are not physical parameters.

The Kolmogorov-Smirnov statistic quantifies a distance between the empirical distribution functions of two samples. Like the desert sand, the Keziluoyi plots between the Pamir-derived Kashgar and the upper Hotan Rivers. This implies that at least some parts of the northern plateau and the Pamir were already exposed between 24 and 30 Ma.

The overlying Anjuan Formation shows a strong provenance change, with a sharp increase in grains <100 Ma as well as the appearance of a significant 690–900 Ma population. New sources must have been exposed by that time (24 to <18 Ma), and this older zircon population indicates that these may have been located within the Pamir. This indicates that an established river drainage from that area must have been established and delivering (significant?) sediment to the southern edge of the Tarim Basin at that time, i.e., the early Miocene. Although Cao et al. (2014) argued that the young (<40 Ma) grains were coming to the Anjuan Formation from the Karakoram via a paleo–Yarkand River, we prefer a source in the western Pamir, based on the closer overall similarity of the U-Pb spectra (Fig. 12) and lack of ca. 60 Ma grains in the Anjuan Formation that are common in the Karakoram (Fig. 8) but absent in the western Pamir and the Anjuan Formation, at least at the 95% confidence level.
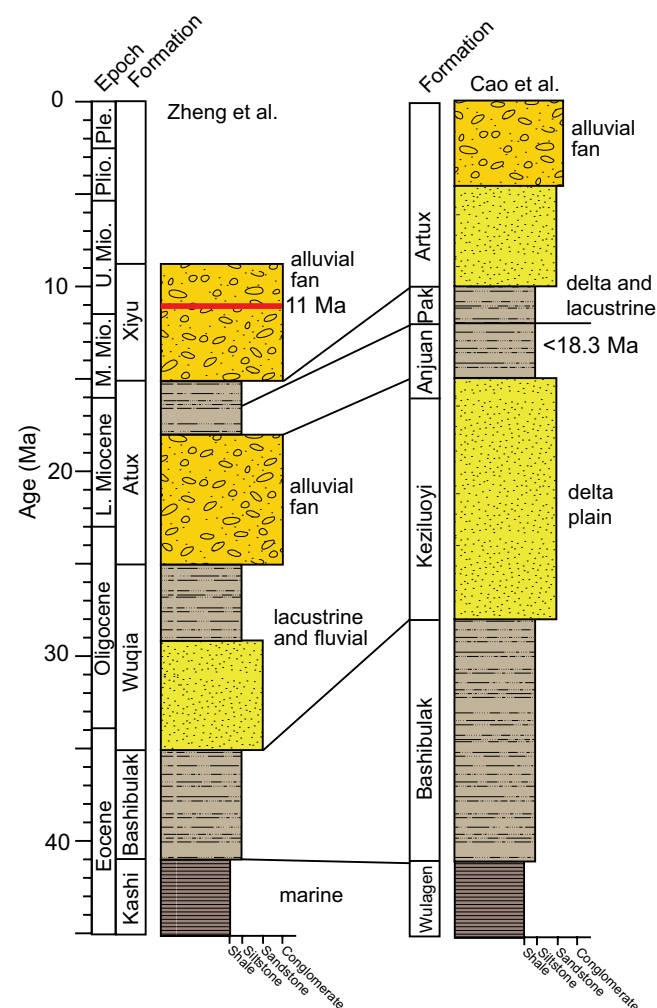
Figure 10. Stratigraphic diagram showing the proposed correlation between the Cenozoic stratigraphy of Zheng et al. (2015) and that of Cao et al. (2014). L.—lower; M.—middle; U.—upper; Mio.—Miocene; Plio.—Pliocene; Ple.—Pleistocene; Pak—Pakabulake.

We think a drainage connection with the Karakoram at that time is unlikely, and we can conclude with confidence that if such a link did exist, then the amount of sediment supplied was very limited. The MDS diagram indicates that the Anjuan Formation has similarity with basement sources in the Cretaceous sedimentary rocks of the Kunlun as well as in the Songpan Garze (Fig. 12). This implies erosion from, sediment delivery from, and thus possible uplift in the
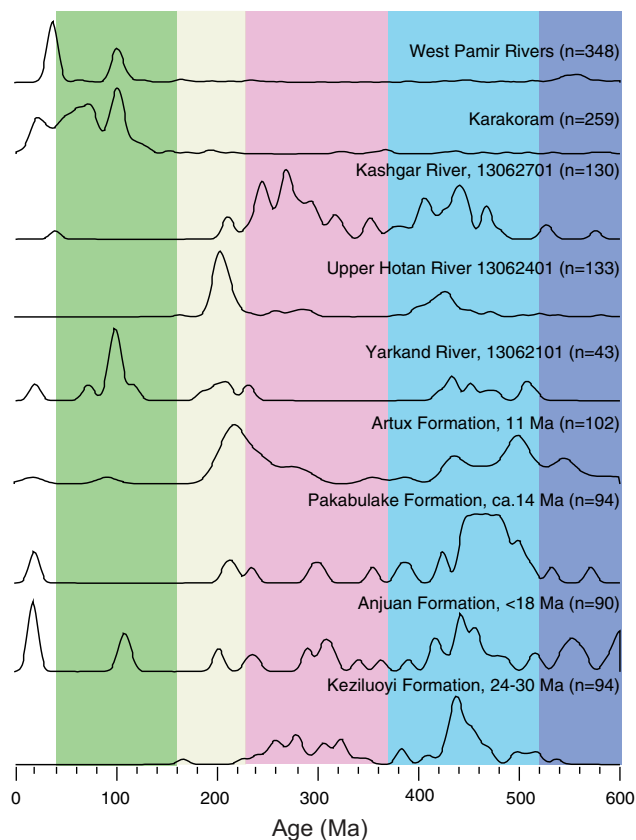
Figure 11. Kernel density estimate plots of zircon U-Pb ages spanning 600 m.y. from the modern samples considered as part of this study compared with detrital zircons from older sedimentary rocks deposited along the northern edge of the Kunlun from Cao et al. (2014). Vertical color bands show defined U-Pb age populations considered to be of use in source discrimination.
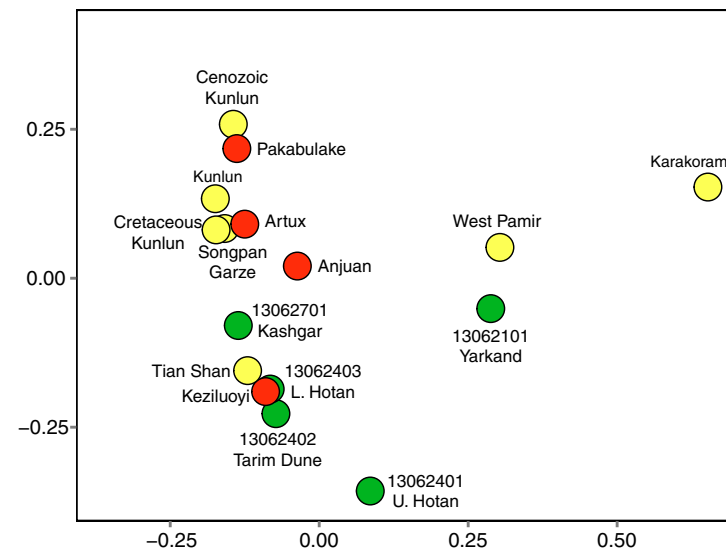

Figure 12. Multidimensional scaling plot showing the Kolmogorov-Smirnov distances between sample zircon age spectra, following the method of Vermeesch (2013). New sediment samples are shown in green and labeled with sample numbers, with possible basement sources in yellow and Cenozoic sedimentary rocks in red. U.—upper; L.—lower.

Kunlun, in addition to that seen in the Pamir at the time of sedimentation. This interpretation is in accord with the Apatite Fission Track (AFT) data from the Hotan River. The western Pamir no longer supply sediment to the Tarim Basin, so some drainage reorganization is required between the western and eastern Pamir since the early Miocene.

The overlying Pakabulake Formation (ca. 14 Ma) is characterized by the disappearance of zircon populations <100 Ma and 230–370 Ma, and another sharp decrease in the relative influence of 690–900 Ma zircons. The source of the Pakabulake Formation would appear to be mostly within the Kunlun and northern Tibetan Plateau, without significant sediment influx from the Pamir. Such a switch is probably at least partly linked to drainage capture away from

the area of sedimentation rather than because the Pamir were not eroding. Comparison between the Pakabulake and overlying Artux Formations shows a significant provenance change between 14 and 11 Ma, particularly with the appearance of a very strong 160–230 Ma population. This is identical to that seen in the modern Hotan River and which we know to be derived from the north Kunlun Block. As a result, we infer the start of sediment flux from the North Kunlun block to the region of the measured sections between 14 and 11 Ma, with the implication that earlier erosion from the Kunlun must have been from the South Kunlun, or even potentially from the Songpan Garze. The appearance of North Kunlun material between 14 and 11 Ma is later than the start of exhumation implied by the ca. 17 Ma AFT age in the Hotan River. This lag may reflect drainage reorganization, with Kunlun sediment being deposited elsewhere between 17 and 11 Ma.

A regional evolution model for the foreland sequence is one of uplift propagating from south to north during the early–middle Miocene with most of the ranges we now see presently in existence by ca. 11 Ma. This is slightly earlier than the middle Miocene to late Miocene uplift implied by Cao et al. (2014) and Wang et al. (2003). It is also noteworthy that no sediment similar to that of the modern Yarkand River is seen in the ancient record, suggesting that this river system is relatively young and that the connection between drainage systems sourcing Karakoram material into the Tarim Basin is a rela-

tively recent development. This is consistent with the observation that grains <100 Ma are not found in Taklimakan Desert sands, which implies minimal delivery from such sources in the geological past.

Regional Exhumation from Apatite Fission-Track Data

Apatite fission-track (AFT) data can be used to look at regional exhumation rates within the drainage of the Hotan River and the sources to the Taklimakan Desert. If we assume a standard range of continental geothermal gradients of 25–30 °C/km and a simple cooling history, then we can use the age population of the sands to estimate average exhumation rates in the sources. The dominant population in the Hotan River clusters at 3.7 ± 0.4 Ma, which implies exhumation rates of 894–1333 m/m.y. if the base of the partial annealing zone is placed at 110 °C (Green, 1989). Our reported central age for the Hotan River is comparable to those reported from the eastern Karakoram at 3.3 ± 0.3 Ma and 7.4 ± 1.1 Ma (Wallis et al., 2016), but is older than those from the central Karakoram around K2 (Foster et al., 1994). Our AFT ages are much younger, and thus exhumation is calculated to be much faster, than in the Transhima-laya and at the southwestern edge of the Tibetan Plateau (Dortch et al., 2011; Kirstein et al., 2006; Munack et al., 2014).

This exhumation rate should reflect the average exhumation rate of North Kunlun bedrock sources that we identified above as the primary supplier to the Hotan River. Although there are two older AFT age populations, these are numerically much smaller and do not dominate the sediment flux. Together our detrital zircon and AFT data indicate that there has been rapid exhumation of at least parts of the North Kunlun since at least 3.7 Ma. However, we also note that there have been moderate rates of exhumation in parts of the Kunlun since ca. 17.3 Ma (185–297 m/m.y.), consistent with basement AFT work (Sobel and Dumitru, 1997), but which occurred still much faster than long-term rates dating back to the Cretaceous. These older AFT ages are not common but do indicate significant regional unroofing back into the mid-Miocene. If these cooling events were triggered by rock uplift, then we could infer that uplift of the North Kunlun initiated by ca. 17 Ma and accelerated no later than 3.7 Ma. The later acceleration is consistent with tilting and facies changes seen in the middle to upper Miocene Xiyu Formation of this area that suggest major uplift starting after ca. 15 Ma (Wang et al., 2003; Zheng et al., 2000).

The AFT ages in the Tarim sands are also dominated by younger ages at ca. 8.1 ± 0.9 Ma, albeit slightly older than those in the Hotan River. This in-dicates that the average source of the Tarim dunes is exhuming a little more slowly than the Kunlun sources of the Hotan River. The combined zircon and Nd-Sr isotope data indicate that the desert sands are from both the Kunlun and the Pamir, which implies that the Pamir sources are exhuming more slowly than the Kunlun in the recent past. Average exhumation rates of the dominant ca. 8.1 Ma dune sand population are ~407–611 m/m.y. Rates are 105–165 m/m.y. for the fission-track age population clustered at ca. 30.8 Ma, if we consider both the uncertainty in the geothermal gradient and the un-certainty in the AFT population ages. Despite the uncertainties, exhumation

rates of the average dunes, and thus the eastern Pamir, are slower than those seen in the Kunlun.

We can also compare these rates with regional exhumation rates in the western Pamir published by Lukens et al. (2012). That study did not include AFT data, but $^{39}Ar/^{40}Ar$ mica dating yielded a young population there of 13–21 Ma. If we use a closure temperature range of 350–420 °C (McDougall and Harrison, 1999) for the mica and our geothermal gradient range of 25–30 °C/km, then we can estimate average exhumation rates of up to 1300 m/m.y. and as low as 560 m/m.y. in the western Pamir. This range is higher than the 407–611 m/m.y. range estimated from the Tarim sands, indicating that the eastern Pamir have been exhuming less rapidly than the western ranges. Furthermore, we note that although Lukens et al. (2012) emphasized that the Pamir are exhuming faster than western Tibet, our data from the Hotan River indicate that at least the North Kunlun are exhuming at comparable rates, i.e., ~894–1333 m/m.y. at least during the Plio-Pleistocene.

Holocene Sediment Transport

Examination of the alluvial terraces in the rivers draining the Kunlun yield a series of rather young valley-filling ages with no clear evidence for other higher and older terraces in the same valleys. In the Kargilik River we see evi-dence for aggradation at ca. 2.6, 1.4, and 0.4 ka. We find that in each case nei-ther the height of the terrace is especially high (<15 m) nor the along-stream extent very great. This suggests that sediment storage within the mountains is not an important factor in buffering the total sediment flux from the moun-tain sources to the depocenter. A regional climatic trigger for valley aggra-dation and incision would explain the relative coincidence of terrace ages in the Kargilik and Kashgar Rivers at ca. 2.5 ka. In the more monsoonal sectors of the Himalaya, valley aggradation is usually associated with an increased sediment supply driven by a strong monsoon (Bookhagen et al., 2006). In this more northern area, the monsoon has less influence and moisture is largely supplied via the Westerlies. This is likely one of the reasons that the strong aggradation recorded in the Himalaya over the early Holocene (10–8 ka) is not observed in this region. Climate records from western China are reflective of a complicated history, although some would argue for a dry and warm phase between 11 and ca. 7 ka followed by warm and wet phase between 7 and 4 ka, and that followed in turn by a fluctuating cool and dry period (Feng et al., 2006). However, such syntheses cover very wide areas with regional differ-ences between the Kunlun and the Tian Shan being lost.

A typical view is that the Tarim Basin experienced a Holocene climatic op-timum between 8 and ca. 5 ka that is not so different from the situation in the western Himalaya (Dixit et al., 2014; Wünnemann et al., 2010). However, there is a lack of agreement on the climatic evolution in western China. A study by Hartmann and Wünnemann (2009) from a lake deposit north of the Tarim Basin argued for an episode of dry conditions between 7.5 and 5.4 ka. This is followed by greater runoff and wetter conditions after 5.4 ka, with the final phase of drying after 4.0 ka. This lake record seems to indicate an extremely

variable monsoon within northwestern China over the Holocene as a result of interactions between the Indian summer monsoon and the winter Westerly Jet. Observations in the recent historical past indicate that the Asian summer monsoon is typically responsible for extreme rainfall events that are more likely to result in sediment transport in the Tarim Basin (Yatagai and Yasunari, 1998). Holmes et al. (2009) summarized proxy data over the Holocene from ice cores, tree rings, and lacustrine sediments that confirmed significant variability in climate both across the region and with altitude. Wünnemann et al. (2006) compiled lake records from this area and were able to identify times of significant desiccation, which they were able to date in the more recent past at 2.6–2.5, 1.9–1.1, and 0.5–0.3 ka, close to the ages of our terrace sediments from the Kargilik River.

Given the age uncertainties in the OSL dating (Table 3), it is not clear whether the valley aggradation was associated with wet periods or the drier intervals because both types of intervals were quite short lived. It is presumed that aggradation is related to increased sediment supply during wetter periods. Terracing is mostly associated with the time of fluctuating climate after 4 ka. Nonetheless, the height and volume of the terraces make it clear that sediment storage in the mountains is not a significant buffer to sediment transport, in stark contrast to the extensive terraces in the Indus River system (Blöthe and Korup, 2013; Clift and Giosan, 2014). In contrast to river systems in more monsoonal areas, there is no suggestion that historic anthropogenic impacts via agricultural disruption have triggered intensified upstream erosion resulting in downstream valley aggradation (Jonell et al., 2016).

Within the Taklimakan Desert itself there are clearly short-term changes in the accretion and deflation of dune complexes. South of the Mazatag Ridge, a significant eolian deposit accumulated ca. 0.5 ka, but this has been deflated in more recent times. This period coincides with the dry period noted by Wünnemann et al. (2006). It is possible that the shift from drier to wet conditions estimated at ca. 0.3 ka may be linked to reorganization of regional winds, which resulted in the change from sediment accretion to erosion in that area. Although the Taklimakan Desert has the potential to be a major sediment buffer over longer time scales, the Holocene record we observe and that is reported in the existing literature indicates rapid sediment recycling over millennial time scales.

■ CONCLUSIONS

Combined radiogenic isotopes and U-Pb dating of detrital zircons from three rivers in the western Tarim Basin reveal the nature of the source terranes and the origin of the sediment in these rivers, as well as those of the dune fields of the Taklimakan Desert. The Yarkand, Hotan, and Kashgar Rivers all show unique provenance signatures. The Yarkand derives much of its sediment from steep, glaciated terrains, largely sourced from the Karakoram near the north flank of K2. This river appears to be relatively new because no sediments with similar U-Pb zircons ages are found within Cenozoic foreland basin strata from

at least ca. 11 Ma. Zircon grains <100 Ma are essentially nonexistent in the Taklimakan Desert sands, implying a low net supply from the Karakoram via a paleo–Yarkand River. A combination of U-Pb zircon and isotope data confirm earlier studies that desert sands are derived largely from a mixture of Kunlun and Pamir sources (Rittner et al., 2016).

The Hotan River derives most of its material from the North Kunlun and shows a population of grains dated at 160–230 Ma that has not yet been discovered in the bedrock of that tectonic block. The Kashgar River appears to be deriving sediment from both the northern and southern flanks of that catchment, although with greater flux from the Tian Shan than from the Pamir. As in the Yarkand, this implies that precipitation is the key process controlling erosion in each river basin, although this is sometimes reinforced by tectonically generated topographic processes.

Apatite fission-track data from the Hotan River and desert dunes indicate rapid exhumation of the North Kunlun since 3.7 Ma following a period of more moderate but still significant exhumation in the middle Miocene, at least by ca. 17 Ma. These rates of exhumation are comparable to those found in the eastern Karakoram (Wallis et al., 2016), and are faster than those of much of the Transhimalaya and western Tibet (Dortch et al., 2011; Kirstein et al., 2006; Munack et al., 2014) but slower than those seen in the central Karakoram (Foster et al., 1994). Apatite fission-track–derived exhumation rates show that the eastern Pamir have been exhuming more slowly than the western Pamir. Examination of the Cenozoic foreland strata reveals a pattern that suggests a northward propagation in uplift and exhumation that is not clearly linked to climatic evolution. The oldest sediments of the Keziluoyi Formation (24–30 Ma) are derived from the Pamir and partly from northern Tibet (Songpan Garze). The subsequent Anjuan Formation, which is younger than 18 Ma, shows erosion from the western Pamir but not the Karakoram as previously believed (Cao et al., 2014), as well as influxes from an uplifting Kunlun block. The overlying Pakabulake Formation (ca. 15 Ma) shows a loss of drainage from the Pamir, suggesting drainage reorganization possibly linked to headwater transfer from the eastern to western Pamir rivers and the re-routing of the Kashgar and associated Pamir rivers toward the north into their present geometries. The uppermost Artux Formation, dated to ca. 11 Ma, is dominated by erosion from the North Kunlun, which was actively uplifting at that time.

Collectively, the data indicate a long and relatively old uplift history for the northwestern margin of the Tibetan Plateau. Most recently, sediment appears to be transported directly from mountain sources into the Taklimakan Desert. Sediment dilution is significant because the rivers themselves recycle desert sediments soon after leaving their rocky headwater gorges, with the original bedrock source signals rapidly diluted as rivers flow farther into the Taklimakan Desert. There is little opportunity for sediment buffering in the headwater regions because of the limited terracing within we find limited terracing within the Kunlun valleys dating at ca. 2.6, 1.4, and 0.5 ka. These late Holocene terraces are unlikely linked to anthropogenic activities but instead reflect changing moisture mostly supplied by extreme South Asian summer monsoon events.

REFERENCES CITED

Aitchison, J.C., Ali, J.R., and Davis, A.S., 2007, When and where did India and Asia collide?: Journal of Geophysical Research, v. 112, B05423, doi:10.1029/2006JB004706.

Avouac, J.P., and Tapponnier, P., 1993, Kinematic model of active deformation in central Asia: Geophysical Research Letters, v. 20, p. 895–898, doi:10.1029/93GL00128.

Bershaw, J., Garzione, C.N., Schoenbohm, L., Gehrels, G., and Tao, L., 2012, Cenozoic evolution of the Pamir plateau based on stratigraphy, zircon provenance, and stable isotopes of foreland basin sediments at Oytag (Wuyitake) in the Tarim Basin (west China): Journal of Asian Earth Sciences, v. 44, p. 136–148, doi:10.1016/j.jseaes.2011.04.020.

Blöthe, J.H., and Korup, O., 2013, Millennial lag times in the Himalayan sediment routing system: Earth and Planetary Science Letters, v. 382, p. 38–46, doi:10.1016/j.epsl.2013.08.044.

Bookhagen, B., Fleitmann, D., Nishiizumi, K., Strecker, M.R., and Thiede, R.C., 2006, Holocene monsoonal dynamics and fluvial terrace formation in the northwest Himalaya, India: Geology, v. 34, p. 601–604, doi:10.1130/G22698.1.

Bosboom, R.E., Dupont-Nivet, G., Houben, A.J.P., Brinkhuis, H., Villa, G., Mandic, O., Stoica, M., Zachariasse, W.-J., Guo, Z., and Li, C., 2011, Late Eocene sea retreat from the Tarim Basin (west China) and concomitant Asian paleoenvironmental change: Palaeogeography, Palaeoclimatology, Palaeoecology, v. 299, p. 385–398, doi:10.1016/j.palaeo.2010.11.019.

Böthe, O., Fraedrich, K., and Zhu, X., 2012, Precipitation climate of Central Asia and the large-scale atmospheric circulation: Theoretical and Applied Climatology, v. 108, p. 345–354, doi:10.1007/s00704-011-0537-2.

Boulin, J., 1988, Hercynian and Eocimmerian events in Afghanistan and adjoining regions: Tectonophysics, v. 148, p. 253–278, doi:10.1016/0040-1951(88)90134-5.

Burbank, D.W., Blythe, A.E., Putkonen, J., Pratt-Sitaula, B., Gabet, E., Oskins, M., Barros, A., and Ojha, T.P., 2003, Decoupling of erosion and precipitation in the Himalayas: Nature, v. 426, p. 652–655, doi:10.1038/nature02187.

Burtman, V.S., and Molnar, P., 1993, Geological and Geophysical Evidence for Deep Subduction of Continental Crust Beneath the Pamir: Geological Society of America Special Paper 281, 76 p., doi:10.1130/SPE281-p1.

Cao, K., Xu, Y., Wang, G., Zhang, K., van der Beek, P., Wang, C., Jiang, S., and Bershaw, J., 2014, Neogene source-to-sink relations between the Pamir and Tarim Basin: Insights from stratigraphy, detrital zircon geochronology, and whole-rock geochemistry: The Journal of Geology, v. 122, p. 433–454, doi:10.1086/676478.

Chang, Q., Mishima, T., Yakubi, S., Takahashi, Y., and Shimizu, H., 2000, Sr and Nd isotope ratios and REE abundances of moraines in the mountain areas surrounding the Taklimakan Desert, NW China: Geochemical Journal, v. 34, p. 407–427, doi:10.2343/geochemj.34.407.

Clift, P.D., and Giosan, L., 2014, Sediment fluxes and buffering in the post-glacial Indus Basin: Basin Research, v. 25, p. 369–386, doi:10.1111/bre.12038.

Clift, P.D., Campbell, I.H., Pringle, M.S., Carter, A., Zhang, X., Hodges, K.V., Khan, A.A., and Allen, C.M., 2004, Thermochronology of the modern Indus River bedload: New insight into the control on the marine stratigraphic record: Tectonics, v. 23, TC5013, doi:10.1029/2003TC001559.

Clift, P.D., Hodges, K., Heslop, D., Hannigan, R., Hoang, L.V., and Calves, G., 2008, Greater Himalayan exhumation triggered by Early Miocene monsoon intensification: Nature Geoscience, v. 1, p. 875–880, doi:10.1038/ngeo351.

Dadson, S., Hovius, N., Chen, H., Dade, W.B., Hsieh, M.-L., Willett, S., Hu, J.-C., Horng, M.-J., Chen, M.-C., Stark, C.P., Lague, D., and Lin, J.-C., 2003, Links between erosion, runoff variability and seismicity in the Taiwan orogen: Nature, v. 426, p. 648–651, doi:10.1038/nature02150.

DePaolo, D.J., and Wasserburg, G.J., 1976, Nd isotopic variations and petrogenetic models: Geophysical Research Letters, v. 3, p. 249–252, doi:10.1029/GL003i005p00249.

Derry, L.A., and France-Lanord, C., 1996, Neogene Himalayan weathering history and river $^{87}Sr/^{86}Sr$: Impact on the marine Sr record: Earth and Planetary Science Letters, v. 142, p. 59–74, doi:10.1016/0012-821X(96)00091-X.

Dickinson, W.R., Beard, S.L., Brackenridge, G.R., Erjavec, J.L., Ferguson, R.C., Inman, K.F., Knepp, R.A., Lindberg, F.A., and Ryber, P.T., 1983, Provenance of North American Phanerozoic sandstones in relation to tectonic setting: Geological Society of America Bulletin, v. 94, p. 222–235, doi:10.1130/0016-7606(1983)94<222:PONAPS>2.0.CO;2.

Dixit, Y., Hodell, D.A., and Petrie, C.A., 2014, Abrupt weakening of the summer monsoon in northwest India ~4100 yr ago: Geology, v. 42, p. 339–342, doi:10.1130/G35236.1.

Dortch, J.M., Dietsch, C., Owen, L.A., Caffee, M.W., and Ruppert, K., 2011, Episodic fluvial incision of rivers and rock uplift in the Himalaya and Transhimalaya: Journal of the Geological Society, v. 168, p. 783–804, doi:10.1144/0016-76492009-158.

Duvall, A.R., Clark, M.K., Avdeev, B., Farley, K.A., and Chen, Z., 2012, Widespread late Cenozoic increase in erosion rates across the interior of eastern Tibet constrained by detrital low-temperature thermochronometry: Tectonics, v. 31, TC3014, doi:10.1029/2011TC002969.

Fedo, C.M., Nesbitt, H.W., and Young, G.M., 1995, Unraveling the effects of potassium metasomatism in sedimentary rocks and paleosols, with implications for paleoweathering conditions and provenance: Geology, v. 23, p. 921–924, doi:10.1130/0091-7613(1995)023<0921:UTEOPM>2.3.CO;2.

Feng, Z.-D., An, C.B., and Wang, H.B., 2006, Holocene climatic and environmental changes in the arid and semi-arid areas of China: A review: The Holocene, v. 16, p. 119–130, doi:10.1191/0959683606hl912xx.

Foster, D.A., Gleadow, A.J.W., and Mortimer, G., 1994, Rapid Pliocene exhumation in the Karakoram (Pakistan), revealed by fission-track thermochronology of the K2 gneiss: Geology, v. 22, p. 19–22, doi:10.1130/0091-7613(1994)022<0019:RPEITK>2.3.CO;2.

Fuchs, M., and Owen, L.A., 2008, Luminescence dating of glacial and associated sediments: Review, recommendations and future directions: Boreas, v. 37, p. 636–659, doi:10.1111/j.1502-3885.2008.00052.x.

Galbraith, R.F., 1990, The radial plot: Graphical assessment of spread in ages: Nuclear Tracks and Radiation Measurements, v. 17, p. 207–214, doi:10.1016/1359-0189(90)90036-W.

Galbraith, R.F., and Roberts, R.G., 2012, Statistical aspects of equivalent dose and error calculation and display in OSL dating: An overview and some recommendations: Quaternary Geochronology, v. 11, p. 1–27.

Garçon, M., Chauvel, C., France-Lanord, C., Huyghe, P., and Lavé, J., 2013, Continental sedimentary processes decouple Nd and Hf isotopes: Geochimica et Cosmochimica Acta, v. 121, p. 177–195, doi:10.1016/j.gca.2013.07.027.

Garçon, M., Chauvel, C., France-Lanord, C., Limonta, M., and Garzanti, E., 2014, Which minerals control the Nd–Hf–Sr–Pb isotopic compositions of river sediments?: Chemical Geology, v. 364, p. 42–55, doi:10.1016/j.chemgeo.2013.11.018.

Garzanti, E., Andó, S., France-Lanord, C., Censi, P., Vignola, P., Galy, V., and Lupker, M., 2011, Mineralogical and chemical variability of fluvial sediments 2. Suspended-load silt (Ganga–Brahmaputra, Bangladesh): Earth and Planetary Science Letters, v. 302, p. 107–120, doi:10.1016/j.epsl.2010.11.043.

Gehrels, G.E., 2014, Detrital zircon U-Pb geochronology applied to tectonics: Annual Review of Earth and Planetary Sciences, v. 42, p. 127–149, doi:10.1146/annurev-earth-050212-124012.

Goldstein, S.L., O'Nions, R.K., and Hamilton, P.J., 1984, A Sm-Nd isotopic study of atmospheric dusts and particulates from major river systems: Earth and Planetary Science Letters, v. 70, p. 221–236, doi:10.1016/0012-821X(84)90007-4.

Green, P.F., 1989, Thermal and tectonic history of the East Midlands shelf (onshore UK) and surrounding regions assessed by apatite fission track analysis: Journal of the Geological Society, v. 146, p. 755–773, doi:10.1144/gsjgs.146.5.0755.

Hartmann, K., and Wünnemann, B., 2009, Hydrological changes and Holocene climate variations in NW China, inferred from lake sediments of Juyanze palaeolake by factor analyses: Quaternary International, v. 194, p. 28–44, doi:10.1016/j.quaint.2007.06.037.

Holmes, J.A., Cook, E.R., and Yang, B., 2009, Climate change over the past 2000 years in Western China: Quaternary International, v. 194, p. 91–107, doi:10.1016/j.quaint.2007.10.013.

Hubbard, M.S., Grew, E.S., Hodges, K.V., Yates, M.G., and Pertsev, N.N., 1999, Neogene cooling and exhumation of upper-amphibolite-facies 'whiteschists' in the southwest Pamir Mountains, Tajikistan: Tectonophysics, v. 305, p. 325–337, doi:10.1016/S0040-1951(99)00012-8.

Ingersoll, R.V., Bullard, T.F., Ford, R.L., Grimm, J.P., Pickle, J.D., and Sares, S.W., 1984, The effect of grain size on detrital modes: A test of the Gazzi-Dickinson point-counting method: Journal of Sedimentary Petrology, v. 54, p. 103–116, doi:10.1306/212F83B9-2B24-11D7-8648000102C1865D.

Jacobsen, S.B., and Wasserburg, G.J., 1980, Sm-Nd isotopic evolution of chondrites: Earth and Planetary Science Letters, v. 50, p. 139–155, doi:10.1016/0012-821X(80)90125-9.

Jolivet, M., Brunel, M., Seward, D., Xu, Z., Yang, J., Roger, F., Tapponnier, P., Malavieille, J., Arnaud, N., and Wu, C., 2001, Mesozoic and Cenozoic tectonics of the northern edge of the Tibetan plateau: Fission-track constraints: Tectonophysics, v. 343, p. 111–134, doi:10.1016/S0040-1951(01)00196-2.

Jonell, T.N., Clift, P.D., Hoang, L.V., Hoang, T., Carter, A., Wittmann, H., Böning, P., Pahnke, K., and Rittenour, T., 2016, Controls on erosion patterns and sediment transport in a monsoonal, tectonically quiescent drainage, Song Gianh, central Vietnam: Basin Research, v. 29, p. 659–683, doi:10.1111/bre.12199.

Kapp, P., Yin, A., Harrison, T.M., and Ding, L., 2005, Cretaceous-Tertiary shortening, basin development, and volcanism in central Tibet: Geological Society of America Bulletin, v. 117, p. 865–878, doi:10.1130/B25595.1.

Kapp, P., DeCelles, P.G., Gehrels, G.E., Heizler, M., and Ding, L., 2007, Geological records of the Lhasa-Qiangtang and Indo-Asian collisions in the Nima area of central Tibet: Geological Society of America Bulletin, v. 119, p. 917–933, doi:10.1130/B26033.1.

Karim, A., and Veizer, J., 2002, Water balance of the Indus River Basin and moisture source in the Karakoram and western Himalayas: Implications from hydrogen and oxygen isotopes river water: Journal of Geophysical Research, v. 107, 4362, doi:10.1029/2000JD000253.

Kirstein, L.A., Sinclair, H.D., Stuart, F.M., and Dobson, K., 2006, Rapid early Miocene exhumation of the Ladakh batholith, western Himalaya: Geology, v. 34, p. 1049–1052, doi:10.1130/G22857A.1.

Kutzbach, J.E., Prell, W.L., and Ruddiman, W.F., 1993, Sensitivity of Eurasian climate to surface uplift of the Tibetan Plateau: The Journal of Geology, v. 101, p. 177–190, doi:10.1086/648215.

Lukens, C.E., Carrapa, B., Singer, B.S., and Gehrels, G., 2012, Miocene exhumation of the Pamir revealed by detrital geothermochronology of Tajik rivers: Tectonics, v. 31, TC2014, doi:10.1029/2011TC003040.

McDougall, I., and Harrison, T.M., 1999, Geochronology and Thermochronology by the $^{40}Ar/^{39}Ar$ Method: Oxford, UK, Oxford University Press, 269 p.

Molnar, P., England, P., and Martinod, J., 1993, Mantle dynamics, uplift of the Tibetan Plateau, and the Indian Monsoon: Reviews of Geophysics, v. 31, p. 357–396, doi:10.1029/93RG02030.

Munack, H., Korup, O., Resentini, A., Limonta, M., Garzanti, E., Blöthe, J.H., Scherler, D., Wittmann, H., and Kubik, P.W., 2014, Postglacial denudation of western Tibetan Plateau margin outpaced by long-term exhumation: Geological Society of America Bulletin, v. 126, p. 1580–1594, doi:10.1130/B30979.1.

Murphy, M.A., Yin, A., Kapp, P., Harrison, T.M., Ding, L., and Guo, J., 2000, Southward propagation of the Karakoram fault system, southwest Tibet: Timing and magnitude of slip: Geology, v. 28, p. 451–454, doi:10.1130/0091-7613(2000)28<451:SPOTKF>2.0.CO;2.

Murray, A.S., and Wintle, A.G., 2000, Luminescence dating of quartz using an improved single-aliquot regenerative-dose protocol: Radiation Measurements, v. 32, p. 57–73, doi:10.1016/S1350-4487(99)00253-X.

Najman, Y., Appel, E., Boudagher-Fadel, M., Bown, P., Carter, A., Garzanti, E., Godin, L., Han, J., Liebke, U., Oliver, G., Parrish, R., and Vezzoli, G., 2010, Timing of India-Asia collision: Geological, biostratigraphic, and palaeomagnetic constraints: Journal of Geophysical Research, v. 115, B12416, doi:10.1029/2010JB007673.

Nesbitt, H.W., Markovics, G., and Price, R.C., 1980, Chemical processes affecting alkalis and alkaline earths during continental weathering: Geochimica et Cosmochimica Acta, v. 44, p. 1659–1666, doi:10.1016/0016-7037(80)90218-5.

Peltzer, G., and Tapponnier, P., 1988, Formation and evolution of strike-slip faults, rifts, and basins during the India-Asia Collision: An experimental approach: Journal of Geophysical Research, v. 93, p. 15,085–15,117, doi:10.1029/JB093iB12p15085.

Phillips, R.J., Parrish, R.R., and Searle, M.P., 2004, Age constraints on ductile deformation and long-term slip rates along the Karakoram fault zone, Ladakh: Earth and Planetary Science Letters, v. 226, p. 305–319, doi:10.1016/j.epsl.2004.07.037.

Prescott, J.R., and Hutton, J.T., 1994, Cosmic ray contributions to dose rates for luminescence and ESR dating: Large depths and long-term time variations: Radiation Measurements, v. 23, p. 497–500, doi:10.1016/1350-4487(94)90086-8.

Ravikant, V., Wu, F.Y., and Ji, W.Q., 2009, Zircon U-Pb and Hf isotopic constraints on petrogenesis of the Cretaceous–Tertiary granites in eastern Karakoram and Ladakh, India: Lithos, v. 110, p. 153–166, doi:10.1016/j.lithos.2008.12.013.

Reiners, P.W., Ehlers, T.A., Mitchell, S.G., and Montgomery, D.R., 2003, Coupled spatial variations in precipitation and long-term erosion rates across the Washington Cascades: Nature, v. 426, p. 645–647, doi:10.1038/nature02111.

Rhodes, E.J., 2011, Optically stimulated luminescence dating of sediments over the past 200,000 years: Annual Review of Earth and Planetary Sciences, v. 39, p. 461–488, doi:10.1146/annurev-earth-040610-133425.

Rittenour, T.M., 2008, Luminescence dating of fluvial deposits: Applications to geomorphic, palaeoseismic and archaeological research: Boreas, v. 37, p. 613–635, doi:10.1111/j.1502-3885.2008.00056.x.

Rittner, M., Vermeesch, P., Carter, A., Bird, A., Stevens, T., Garzanti, E., Andò, S., Vezzoli, G., Dutt, R., Xu, Z., and Lu, H., 2016, The provenance of Taklamakan desert sand: Earth and Planetary Science Letters, v. 437, p. 127–137, doi:10.1016/j.epsl.2015.12.036.

Robinson, A.C., Yin, A., Manning, C.E., Harrison, T.M., Zhang, S.-H., and Wang, X.-F., 2004, Tectonic evolution of the northeastern Pamir: Constraints from the northern portion of the Cenozoic Kongur Shan extensional system, western China: Geological Society of America Bulletin, v. 116, p. 953–973, doi:10.1130/B25375.1.

Robinson, A.C., Yin, A., Manning, C.E., Harrison, T.M., Zhang, S.-H., and Wang, X.-F., 2007, Cenozoic evolution of the eastern Pamir: Implications for the strain-accommodation mechanisms at the western end of the Himalayan-Tibetan orogen: Geological Society of America Bulletin, v. 119, p. 882–896, doi:10.1130/B25981.1.

Robinson, A.C., Ducea, M., and Lapen, T.J., 2012, Detrital zircon and isotopic constraints on the crustal architecture and tectonic evolution of the northeastern Pamir: Tectonics, v. 31, TC2016, doi:10.1029/2011TC003013.

Schärer, U., Copeland, P., Harrison, T.M., and Searle, M.P., 1990, Age, cooling history, and origin of post-collisional leucogranites in the Karakoram Batholith: A multi-system isotope study: The Journal of Geology, v. 98, p. 233–251, doi:10.1086/629395.

Schulz, H.-M., Bechtel, A., and Sachsenhofer, R.F., 2005, The birth of the Paratethys during the Early Oligocene: From Tethys to an ancient Black Sea analogue?: Global and Planetary Change, v. 49, p. 163–176, doi:10.1016/j.gloplacha.2005.07.001.

Searle, M.P., 1991, Geology and Tectonics of the Karakoram Mountains: Chichester, UK, John Wiley and Sons, 358 p.

Searle, M.P., and Phillips, R.J., 2007, Relationships between right-lateral shear along the Karakoram fault and metamorphism, magmatism, exhumation and uplift: Evidence from the K2-Gasherbrum-Pangong ranges, north Pakistan and Ladakh: Journal of the Geological Society, v. 164, p. 439–450, doi:10.1144/0016-76492006-072.

Searle, M.P., Parrish, R.R., Tirrul, R., and Rex, D.C., 1990, Age of crystallization of the K2 gneiss in the Baltoro Karakoram: Journal of the Geological Society, v. 147, p. 603–606, doi:10.1144/gsjgs.147.4.0603.

Searle, M.P., Rex, A.J., Tirrul, R., Rex, D.C., Barnicoat, A., and Windley, B.F., 1989, Metamorphic, magmatic, and tectonic evolution of the central Karakoram in the Biafo-Baltoro-Hushe regions of north Pakistan, in Malinconico, L.L., Jr., and Lillie, R.J., eds., Tectonics of the Western Himalayas: Geological Society of America Special Paper 232, p. 47–74, doi:10.1130/SPE232-p47.

Sengor, A.M.C., and Natal'in, B.A., 1996, Paleotectonics of Asia: Fragments of a synthesis, in Yin, A., and Harrison, M., eds., The Tectonic Evolution of Asia: Cambridge, UK, Cambridge University Press, p. 486–640.

Shao, Y., Wyrwoll, K.-H., Chappell, A., Huang, J., Lin, Z., McTainsh, G.H., Mikami, M., Tanaka, T.Y., Wang, X., and Yoon, S., 2011, Dust cycle: An emerging core theme in Earth system science: Aeolian Research, v. 2, p. 181–204, doi:10.1016/j.aeolia.2011.02.001.

She, Z., Ma, C., Mason, R., Li, J., Wang, G., and Lei, Y., 2006, Provenance of the Triassic Songpan–Ganzi flysch, west China: Chemical Geology, v. 231, p. 159–175, doi:10.1016/j.chemgeo.2006.01.001.

Sobel, E.R., and Dumitru, T.A., 1997, Thrusting and exhumation around the margins of the western Tarim basin during the India-Asia collision: Journal of Geophysical Research, v. 102, p. 5043–5063, doi:10.1029/96JB03267.

Sobel, E.R., Chen, J., and Heermance, R.V., 2006a, Late Oligocene–Early Miocene initiation of shortening in the Southwestern Chinese Tian Shan: Implications for Neogene shortening rate variations: Earth and Planetary Science Letters, v. 247, p. 70–81, doi:10.1016/j.epsl.2006.03.048.

Sobel, E.R., Oskin, M., Burbank, D., and Mikolaichuk, A., 2006b, Exhumation of basement-cored uplifts: Example of the Kyrgyz Range quantified with apatite fission track thermochronology: Tectonics, v. 25, TC2008. doi:10.1029/2005TC001809.

Sun, J., Xiao, W., Windley, B.F., Ji, W., Fu, B., Wang, J., and Jin, C., 2016, Provenance change of sediment input in the northeastern foreland of Pamir related to collision of the Indian

Plate with the Kohistan-Ladakh arc at around 47 Ma: Tectonics, v. 35, p. 315–338, doi:10.1002/2015TC003974.

Tada, R., Zheng, H., Sugiura, N., Isozaki, Y., Hasegawa, H., Sun, Y., Yang, W., Wang, K., and Toyoda, S., 2010, Desertification and dust emission history of the Tarim Basin and its relation to the uplift of northern Tibet, in Clift, P.D., Tada, R., and Zheng, H., eds., Monsoon Evolution and Tectonics–Climate Linkage in Asia: Geological Society of London Special Publication 342, p. 45–65, doi:10.1144/SP342.5.

Tada, R., Zheng, H., and Clift, P.D., 2016, Evolution and variability of the Asian monsoon and its potential linkage with uplift of the Himalaya and Tibetan Plateau: Progress in Earth and Planetary Science, v. 3, 4, doi:10.1186/s40645-016-0080-y.

Tang, W., Zhang, Z., Li, J., Li, K., Luo, Z., and Chen, Y., 2015, Mesozoic and Cenozoic uplift and exhumation of the Bogda Mountain, NW China: Evidence from apatite fission track analysis: Geoscience Frontiers, v. 6, p. 617–625, doi:10.1016/j.gsf.2014.04.006.

Tapponnier, P., Mattauer, M., Proust, F., and Cassaigneau, C., 1981, Mesozoic ophiolites, sutures, and large-sale tectonic movements in Afghanistan: Earth and Planetary Science Letters, v. 52, p. 355–371, doi:10.1016/0012-821X(81)90189-8.

Tapponnier, P., Zhiqin, X., Roger, F., Meyer, B., Arnaud, N., Wittlinger, G., and Jingsui, Y., 2002, Oblique stepwise growth of the Tibet Plateau: Science, v. 294, p. 1671–1677, doi:10.1126/science.105978.

Uno, I., Eguchi, K., Yumimoto, K., Takemura, T., Shimizu, A., Uematsu, M., Liu, Z., Wang, Z., Hara, Y., and Sugimoto, N., 2009, Asian dust transported one full circuit around the globe: Nature Geoscience, v. 2, p. 557–560, doi:10.1038/ngeo583.

Vermeesch, P., 2004, How many grains are needed for a provenance study?: Earth and Planetary Science Letters, v. 224, p. 441–451, doi:10.1016/j.epsl.2004.05.037.

Vermeesch, P., 2013, Multi-sample comparison of detrital age distributions: Chemical Geology, v. 341, p. 140–146, doi:10.1016/j.chemgeo.2013.01.010.

Wallis, D., Carter, A., Phillips, R.J., Parsons, A.J., and Searle, M.P., 2016, Spatial variation in exhumation rates across Ladakh and the Karakoram: New apatite fission track data from the Eastern Karakoram, NW India: Tectonics, v. 35, p. 704–721, doi:10.1002/2015TC003943.

Wang, E., Wan, J., and Liu, J., 2003, Late Cenozoic geological evolution of the foreland basin bordering the West Kunlun range in Pulu area: Constraints on timing of uplift of northern margin of the Tibetan Plateau: Journal of Geophysical Research, v. 108, 2401, doi:10.1029/2002JB001877.

Wang, E., Kirby, E., Furlong, K.P., van Soest, M., Xu, G., Shi, X., Kamp, P.J.J., and Hodges, K.V., 2012, Two-phase growth of high topography in eastern Tibet during the Cenozoic: Nature Geoscience, v. 5, p. 640–645, doi:10.1038/ngeo1538.

Weislogel, A.L., Graham, S.A., Chang, E.Z., Wooden, J.L., and Gehrels, G., 2010, Detrital zircon provenance from three turbidite depocenters of the Middle-Upper Triassic Songpan-Ganzi complex, central China: Record of collisional tectonics, erosional exhumation, and sediment production: Geological Society of America Bulletin, v. 122, p. 2041–2062, doi:org/10.1130/B26606.1.

Whipple, K.X., 2009, The influence of climate on the tectonic evolution of mountain belts: Nature Geoscience, v. 2, p. 97–104, doi:10.1038/ngeo413.

Wobus, C.W., Hodges, K.V., and Whipple, K.X., 2003, Has focused denudation sustained active thrusting at the Himalayan topographic front?: Geology, v. 31, p. 861–864, doi:10.1130/G19730.1.

Wünnemann, B., Mischke, S., and Chen, F., 2006, A Holocene sedimentary record from Bosten Lake, China: Palaeogeography, Palaeoclimatology, Palaeoecology, v. 234, p. 223–238, doi:10.1016/j.palaeo.2005.10.016.

Wünnemann, B., Demske, D., Tarasov, P., Kotlia, B.S., Reinhardt, C., Bloemendal, J., Diekmann, B., Hartmann, K., Krois, J., Riedel, F., and Arya, N., 2010, Hydrological evolution during the last 15 kyr in the Tso Kar lake basin (Ladakh, India), derived from geomorphological, sedimentological and palynological records: Quaternary Science Reviews, v. 29, p. 1138–1155, doi:10.1016/j.quascirev.2010.02.017.

Wyshnytzky, C.E., Rittenour, T.M., Nelson, M.S., and Thackray, G., 2015, Luminescence dating of late Pleistocene proximal glacial sediments in the Olympic Mountains, Washington: Quaternary International, v. 362, p. 116–123, doi:10.1016/j.quaint.2014.08.024.

Yang, S., Zhang, F., and Wang, Z., 2012, Grain size distribution and age population of detrital zircons from the Changjiang (Yangtze) River system, China: Chemical Geology, v. 296–297, p. 26–38, doi:10.1016/j.chemgeo.2011.12.016.

Yang, X., Zhu, B., and White, P.D., 2007, Provenance of aeolian sediment in the Taklamakan Desert of western China, inferred from REE and major-elemental data: Quaternary International, v. 175, p. 71–85, doi:10.1016/j.quaint.2007.03.005.

Yatagai, A., and Yasunari, T., 1998, Variation of summer water vapor transport related to precipitation over and around the arid region in the interior of the Eurasian continent: Journal of the Meteorological Society of Japan, v. 76, p. 799–815, doi:10.2151/jmsj1965.76.5_799.

Yin, A., and Harrison, T.M., 2000, Geologic evolution of the Himalayan-Tibetan orogen: Annual Review of Earth and Planetary Sciences, v. 28, p. 211–280, doi:10.1146/annurev.earth.28.1.211.

Zhang, R., Jiang, D., Zhang, Z., and Yu, E., 2015, The impact of regional uplift of the Tibetan Plateau on the Asian monsoon climate: Palaeogeography, Palaeoclimatology, Palaeoecology, v. 417, p. 137–150, doi:10.1016/j.palaeo.2014.10.030.

Zheng, H., Powell, C.M., An, Z., Zhou, J., and Dong, G., 2000, Pliocene uplift of the northern Tibetan Plateau: Geology, v. 28, p. 715–718, doi:10.1130/0091-7613(2000)28<715:PUOTNT>2.0.CO;2.

Zheng, H., Tada, R., Jia, J., Lawrence, C., and Wang, K., 2010, Cenozoic sediments in the southern Tarim Basin: Implications for the uplift of northern Tibet and evolution of the Taklimakan Desert, in Clift, P. D., Tada, R., and Zheng, H., eds., Monsoon Evolution and Tectonics–Climate Linkage in Asia: Geological Society of London Special Publication 342, p. 67–78, doi:10.1144/SP342.6.

Zheng, H., Wei, X., Tada, R., Clift, P.D., Wang, B., Jourdan, F., Wang, P., and He, M., 2015, Late Oligocene–early Miocene birth of the Taklimakan Desert: Proceedings of the National Academy of Sciences of the United States of America, v. 112, p. 7662–7667, doi:10.1073/pnas.1424487112.